

**CHARACTERIZATION OF A SINGLE PIXEL BETA DETECTOR FOR GUIDANCE IN
BREAST-CONSERVING SURGERY**

by

Amritpal Singh

Post MSc Course in Accelerator Physics, Panjab University, India, 2012

MSc Physics, Panjab University, India, 2008

BSc (General), Panjab University, India, 2006

A thesis

presented to Ryerson University

in partial fulfilment of the

requirements for the degree of

Master of Science

in the Program of

Biomedical Physics

Toronto, Ontario, Canada, 2018

© Amritpal Singh, 2018

AUTHOR'S DECLARATION FOR ELECTRONIC SUBMISSION OF A THESIS

I hereby declare that I am the sole author of this thesis. This is a true copy of the thesis, including any required final revisions, as accepted by my examiners.

I authorize Ryerson University to lend this thesis to other institutions or individuals for the purpose of scholarly research.

I further authorize Ryerson University to reproduce this thesis by photocopying or by other means, in total or in part, at the request of other institutions or individuals for the purpose of scholarly research.

I understand that my thesis may be made electronically available to the public.

Abstract

Characterization of a Single Pixel Beta Detector for Guidance in Breast-conserving Surgery

Amritpal Singh

Master of Science

Biomedical Physics

Ryerson University

2018

Breast-conserving surgery (BCS) is a challenging surgical procedure due to the lack of intra-operative image guidance available to surgeons. One potential method of intra-operative guidance would be radio-guided surgery with radiopharmaceutical emitting beta particles. In this thesis, a single pixel beta sensitive detector was constructed and characterized for intra-operative guidance during BCS. The thickness of the scintillation element of the detector was optimized to obtain a superior beta to gamma detection ratio. A computer model of the detector response was derived from an empirically measured, two-dimensional (2D) detector response. An *in silico* study evaluated whether the novel single pixel beta detector could detect less than 1 mm² deposits of cancer at the cut edge of the surgically excised cancerous tissue, with a sensitivity and specificity of 95%.

A thickness of 0.5 mm for a CaF₂(Eu) scintillator was found to be optimal for a beta to gamma detection ratio. Additionally, according to an *in silico* study it is expected that with an acquisition time of 30 seconds, a tumour-to-background ratio of 5 or higher, and a normal breast tissue activity of 1.69 kBq/ml, detection of cancerous deposits of less than 1 mm² is possible.

The result of this thesis demonstrate that radio-guided BCS, with a CaF₂(Eu) scintillation beta particle detector, can intra-operatively assess the tumour margin involvement, which would help surgeons in determining resection margins.

Acknowledgements

From the very beginning of this project, it was known to me that this research would not have been realized all alone. I have been continuously supported by many people throughout the project. I would like to thank the following people:

First of all I would like to thank my esteemed supervisor, Dr. Ananth Ravi for his endless support and encouragement. I am deeply indebted to him for his critical wisdom and mentorship throughout the years. Dr. Ravi played a pivotal role in the development of my scientific skills. I feel lucky to work under the supervision of a man of uncompromising principles.

I am beholden to my supervisory committee members Dr. Carl Kumaradas, Dr. James Gafe, and Dr. Raffi Karshafian for their much needed feedback on my research work and guiding me to accomplish this research project.

I express my sincere gratitude to Mr. John Dillon for his sincere support throughout the project.

I would like to give my warm thanks to Mr. Harry Easton, who helped me to design different types of hardware required for experiments.

I express my heartiest thanks to my friends Dr. Manmeet Pal Singh and Dr. Krishnan Sathiyamoorthy, who encouraged and supported me throughout this journey.

I would also like to thank Cancer Imaging Network of Ontario for providing financial help for this research project.

I do not have words to express gratitude to my beloved father Mr. Chanan Singh and mother Miss Chanan Kaur. Without their unconditional love and support I could not complete this thesis. I could write another thesis for the love and support of my wife Miss Ravinder Kaur. Her patience and encouragement fuelled me to finish my thesis efficiently, when she was busy raising our kids Avraj Singh and Avitaj Singh, and I was spending more time in the lab than with them.

Table of Contents

Declaration	ii
Abstract	iii
List of Tables	vii
List of Figures	viii
Acronyms.....	ix
Chapter 1 Introduction.....	1
1.1 Breast cancer.....	2
1.1.1 Breast cancer incidence.....	2
1.1.2 Types of breast cancer.....	3
1.1.3 Risk factors	4
1.1.4 Breast cancer staging	5
1.1.5 Prognosis.....	7
1.1.6 Mortality	7
1.2 Breast cancer detection	7
1.2.1 Breast screening	7
1.2.2 Diagnostic mammography	8
1.2.3 Diagnostic ultrasound	8
1.2.4 Magnetic resonance imaging	9
1.3 Breast cancer surgery.....	9
1.4 Pathological evaluation of a surgery	9
1.5. Intra-operative guidance techniques	10
1.5.1 Palpation	10
1.5.2 Wire guided localization	11
1.5.3 Intra-operative sonography (Ultrasound).....	11
1.5.4 Intra-operative radioactive seed localization	12
1.5.5 Radio-guided surgery.....	13
1.6 Definition of the problem.....	16
1.6.1 Hypothesis.....	16
1.6.2 Specific objective.....	17
1.7 Beta particle detection.....	17
1.7.1 Radiation interactions with absorber.....	17

1.7.2 Beta particle detectors	19
1.7.3 Scintillator	20
1.7.4 Photodetector	22
1.7.5 Existing beta scintillation detectors	23
1.8 Newly proposed beta detector and its characterization	24
1.9 Thesis overview	25
Chapter 2 Construction and characterization of a novel single pixel beta detector for intra-operative guidance in breast-conserving surgery	26
2.1 Abstract	27
2.2 Introduction	28
2.3 Methods	30
2.3.1 Beta particle detector	30
2.3.2 Crystal thickness optimization	31
2.3.3 Creating a detector sensitivity map	32
2.3.4 Minimum detectable tumour surface area (MDTSA)	33
2.4 Results	37
2.4.1 Crystal thickness optimization	37
2.4.2 Detector sensitivity map	39
2.4.3 Minimum detectable tumour surface area (MDTSA)	40
2.5 Discussion	42
2.6 Conclusion	44
2.7 Acknowledgements	44
Chapter 3 Conclusion	45
3.1 Thesis overview	46
3.2 Discussion and future work	47
Appendix	49
A1 Tumour Model	49
A2 Tumour growth	49
Bibliography	50

List of Tables

Table 1. TNM staging system of breast cancer according to the AJCC (7th edition)	6
Table 2. Characteristics of beta particle emitting radionuclides which are used or have the potential to be used in beta guided surgeries.	16
Table 3. Properties of organic and inorganic scintillators suitable for beta particles detection. .	21
Table 4. Beta particle sensitive probes/detectors	29
Table 5. Average SUV (SUV_{avg}), mean, and median SUV_{avg} , in normal breast tissue for patients with different breast density and menopausal status.....	35
Table 6. Maximum SUV (SUV_{max}), mean, and median SUV_{max} , in breast tumours for patients who may be eligible for a BCS.	36
Table 7. Comparison of three thicknesses of $CaF_2(Eu)$ crystal in terms of beta to gamma detection ratio.....	37

List of Figures

Figure 1. Age standardized incidence and mortality rates for breast cancer in American women according to the surveillance, epidemiology, and end results database.....	3
Figure 2. Structure of the beta sensitive single pixel detector.	31
Figure 3. Schematic diagram of source geometry.	32
Figure 4. Apparatus used to acquire the sensitivity map of the beta sensitive detector for ^{18}F -FDG radiopharmaceutical.	33
Figure 5. Pictorial representation of the modeled surgically excised tumour and its iterative growth in the breast duct.	36
Figure 6. Overall, photon and beta spectra obtained with three $\text{CaF}_2(\text{Eu})$ crystals by exposing detectors to the ^{18}F -FDG source.	38
Figure 7. Graphical representation of the 2D sensitivity map of the beta sensitive detector.	39
Figure 8. The rapid fall of detector sensitivity with an increase in distance of the source from the detector.....	40
Figure 9. The effect of increasing acquisition time on the MDTSA.	40
Figure 10. The effect of increasing breast normal tissue activity on the MDTSA.	41
Figure 11. The effect of increasing the T:B ratio on the MDTSA.	42

Acronyms

AJCC	American Joint Committee on Cancer
APD	Avalanche photodiode
BCS	Breast-conserving surgery
BGO	Bismuth germanate
CEA	Human carcinoembryonic antigen
2D	Two-Dimensional
3D	Three-Dimensional
DCIS	Ductal carcinoma in situ
CPS	Counts per second
^{18}F	Fluorine-18
^{18}F -FDG	2-Deoxy-2-[^{18}F] Fluoroglucose
GDP	Gamma-ray detection probe
GM-APD	Geiger mode avalanche photodiode
HER-2	Human epidermal growth factor receptor-2
HER-3	Human epidermal growth factor receptor-3
^{125}I	Iodine-125
^{111}I	Iodine-111
IDC	Invasive ductal carcinoma
ILC	Invasive lobular carcinoma

IOUS	Intra-operative ultrasound
LCIS	Lobular carcinoma in situ
Mabs	Monoclonal antibodies
MDTSA	Minimum detectable tumour surface area
MRI	Magnetic resonance imaging
PMT	Photomultiplier tube
PMMA	Polymethyl methacrylate
RIGS	Radio-immuno guided surgery
RGS	Radio-guided surgery
RSL	Radioactive seed localization
SiPM	Silicon photomultiplier
TAA	Tumour associated antigens
T:B	Tumour-to-Background
SUV	Standardized uptake value
SEER	the surveillance, epidemiology, and end results
TAG-72	Tumour associated glycoprotein-72
TNM	Tumour size, nodal involvement, and metastasis
WGL	Wire-guided localization

Chapter 1 Introduction

1.1 Breast cancer

1.1.1 Breast cancer incidence

According to the Canadian Cancer Society (2017), it was estimated that 50% of Canadians will develop cancer in their lifetime and one in four Canadians will die of this disease. It was estimated that in 2017, 206,200 Canadians would develop cancer, of which 50% would be lung, breast, colorectal, and prostate cancer [1]. Accounting for 13% of all cancer cases and 25% of female cancer cases, breast cancer is the most common type of cancer in females [1,2]. One in eight Canadian women are expected to develop breast cancer during their lifetime [1].

Breast cancer incidence rates increased sharply in the beginning of the 1990s [1]. The sudden rise in incidence rates could be attributed to the diagnosis of breast cancer in earlier stages due to improvement in medical imaging and the advent of screening mammography. The number of women over the age of 50 years having mammograms increased from 40% in 1990 to 72% in 2000 [3]. Figure 1 represents age standardized incidence and mortality rates in American women according to the surveillance, epidemiology, and end results (SEER) statistics. These rates are in line with breast cancer patients in Canada. Figure 1 also represents a sharp increase in the number of patients with carcinoma in situ in the 1990s.

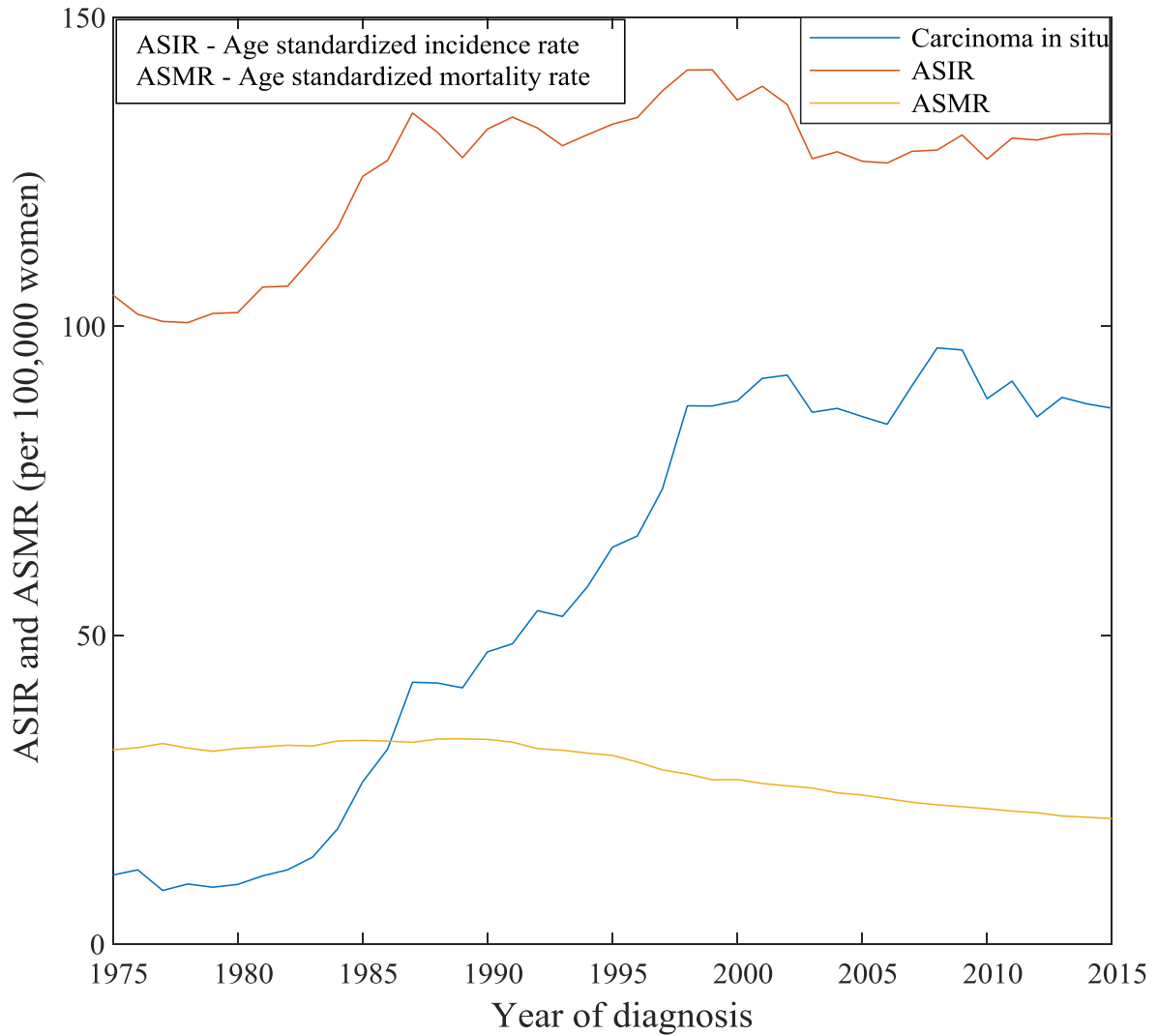


Figure 1. Age standardized incidence and mortality rates for breast cancer in American women according to the surveillance, epidemiology, and end results database.

1.1.2 Types of breast cancer

Breast cancer is a group of different kinds of cancer that influence the breast. Types of breast cancer include non-invasive, invasive, inflammatory and paget's disease of nipple discharge.

1.1.2.1 Non-invasive breast cancer

Non-invasive breast cancers remain within milk ducts or lobules, and they do not spread to the other breast tissue. The cancer that is confined within the milk duct is referred as ductal carcinoma in situ (DCIS), whereas, the cancer that stays within the lobule is termed as lobular carcinoma in situ (LCIS) [4].

1.1.2.2 Invasive breast cancer

This is a breast cancer that invades healthy breast tissue surrounding the place from where it began. Invasive ductal carcinoma (IDC) is a commonly diagnosed breast cancer. Approximately, 80% breast cancer cases are IDC [4]. It begins from a milk duct, emerges out of the duct wall, and spreads to the other breast tissue. On the other hand invasive lobular carcinoma (ILC) is a less common invasive breast cancer. Approximately, 10% of breast cancer cases are ILC [4]. It starts in lobules and grows into the surrounding healthy tissue.

1.1.2.3 Inflammatory breast cancer

Inflammatory breast cancer starts from milk ducts and spreads to lymph vessels. It is less common, but an aggressive form of breast cancer. It accounts for less than 3% breast cancer cases [4].

1.1.2.4 Paget's disease of nipple

Paget's disease of nipple results in cancer cells proliferation in and around the nipple. This is a rarely diagnosed form of breast cancer, which accounts for approximately 5% of all breast cancer cases [4].

1.1.3 Risk factors

Breast cancer is a common type of cancer diagnosed in women. Breast cancer etiology is not completely understood. Known risk factors account for a small fraction of breast cancers. However, main factors that influence the beginning of breast cancer are:

1. Gender: Breast cancer is more pronounced in women. The female to male breast cancer patient ratio is 100:1 [5].
2. Age: Breast cancer risk increases with age. Until menopause, the breast cancer incidence rate doubles every ten years [6]. Within Canada 52% of breast cancer patients are in the age group of 50-69 years, whereas only 18% of patients are below 50 years of age [1].

3. Geographical Variation: Breast cancer incidence is approximately four times higher in Western Europe compared to Middle Africa and Eastern Asia [2].
4. Reproductive events: Women with one or more pregnancies, first pregnancy at a young age (≤ 24 years) are at a lower risk of breast cancer compared to nulliparous women [7,8]. Also women who have breastfed are at reduced risk of breast cancer [8].
5. Hormone-related factors: Early menarche is a responsible factor for increased breast cancer risk [7]. Moreover, women who entered menopause at 45 years of age or older are at increased risk compared to women who entered menopause before 45 years of age [6,9].
6. Ionizing radiation: The exposure to ionizing radiation elevates the breast cancer risk. The radiation dose absorbed in the breast during a chest CT scan and radiotherapy has shown an increase in breast cancer risk [10].
7. Family history and genetic factors: Family history modulates breast cancer risk factors. In Western countries, 10% of breast cancer patients have a history of cancer in their parents [6]. Moreover, inherited genes may also contribute to the increased breast cancer risk. It is expected that 7% of all breast cancer cases are due to inherited genes from parents [5]. Additionally, a woman with her mother affected from breast cancer is at three-fold risk of developing cancer [11].

Furthermore, diabetes [12], alcohol consumption [13], and smoking [14] significantly increase the breast cancer risk.

1.1.4 Breast cancer staging

Breast cancer staging is a clinical description of the disease extent. It is done by using the internationally accepted tumour, node, metastasis (TNM) staging system developed by the American Joint Committee on Cancer (AJCC). This system classifies the cancer stages on the basis of the anatomical spread of cancer cells. It is the most important prognostic indicator used to guide treatment in patients. After the staging, the physician can address the patient for treatment issues and treatment options such as breast-conserving therapy, mastectomy, radiation therapy. Breast cancer staging or breast tumour classification, in terms of combined TNM mapping, is described in Table 1.

Table 1. TNM staging system of breast cancer according to the AJCC (7th edition)

Malignancy Stage	TNM status	Description
Stage 0	Tis, N0, M0	Carcinoma in situ, no nodal involvement, no metastasis.
Stage IA	T1, N0, M0	Greatest tumour diameter ≤ 2 cm, no nodal involvement, no metastasis.
Stage IB	T0, N1mi, M0	No evidence of primary tumour, micrometastasis to axillary lymph nodes.
	T1, N1mi, M0	Greatest Tumour diameter ≤ 2 cm, micrometastasis to axillary lymph nodes.
Stage IIA	T0, N1, M0	No evidence of primary tumour, ≤ 3 axillary lymph nodes, internal mammary lymph nodes or both involved.
	T1, N1, M0	Greatest tumour diameter ≤ 2 cm, ≤ 3 axillary lymph nodes, internal mammary lymph nodes or both involved
Stage IIB	T2, N0, M0	Tumour is > 2 cm and ≤ 5 cm in greatest diameter
	T2, N1, M0	Tumour is > 2 cm and ≤ 5 cm in greatest diameter, ≤ 3 axillary lymph nodes, internal mammary lymph nodes or both involved.
Stage IIIA	T3, N0, M0	Tumour size > 5 cm (greatest diameter).
	T3, N1, M0 T0-3, N2, M0	Tumour of any size, ≤ 9 axillary lymph nodes or internal mammary lymph nodes or ≤ 3 axillary lymph nodes and internal mammary lymph nodes involved.
Stage IIIB	T4, N0-2, M0	A tumour extends to muscles of the chest wall or skin or both, ≤ 9 axillary lymph nodes or internal mammary lymph nodes involved or ≤ 3 axillary lymph nodes and internal mammary lymph nodes involved.
StageIIIC	Any T, N3, M0	Cancer spreads to infraclavicular lymph nodes
Stage IV	Any T, Any N, M1	Distant metastasis present.

1.1.5 Prognosis

A prognosis is an estimate of the effect of the cancer and its treatment on patient. A breast cancer prognosis depends on many factors such as cancer stage, cancer spread to lymph nodes, tumour size, and tumour grade. The breast cancer stage is a most important prognostic factor for the breast cancer patient. The early stage breast cancer possess a less risk of recurrence. Breast cancer detected at a later stage has a less favourable prognosis. According to the SEER database, five-year survival rates are approximately 100%, 93%, 72%, and 22%, for the stage I, stage II, stage III, and stage IV breast cancer, respectively [15]. Similar results were reported by other studies as well [16,17].

1.1.6 Mortality

According to the Canadian Cancer Society (2017), it was expected that 80,800 Canadians would die of cancer in 2017. In women, breast cancer is the second most common cause of cancer deaths after lung cancer, constituting 13% of overall cancer deaths in Canadian females. Moreover, an estimated 1 in 31 women in Canada dies of breast cancer annually. Female breast cancer death rate peaked in 1986 at 41.7 deaths per 100,000 women, and dropped by 44% to 23.2 deaths per 100,000 women in 2017 [1]. This significant fall in the mortality rate is attributed to the improvements in the early-stage breast cancer detection through screening [18], and the introduction of the adjuvant chemotherapy and the hormonal therapy [19].

1.2 Breast cancer detection

1.2.1 Breast screening

Periodic breast screening is performed as a regular checkup after a certain age in females. Breast screening results in the detection of the disease, before any type of physical or clinical symptoms of breast cancer occur. Moreover, the early detection of breast cancer increases the chance of successful treatment and reduces the risk of metastasis.

Mammography is commonly used for breast screening. It uses low energy X-rays to image the internal structure of the breast. Screening x-ray mammography has a sensitivity of up to 93% for detecting breast cancer [20,21]. However, sensitivity of screening mammography decreases with increasing breast density. It drops from 80% among women with non-dense breast to 30% in extremely dense breast tissue [21]. It is hypothesized that the use of

ultrasonography, as an adjunct to mammography, is beneficial in breast screening [22]. According to Buchberger et al., combined screening with mammography and ultrasound increases the detection sensitivity to 81.3% compared to 61.5% with mammography alone in women with dense breasts [23]. Moreover, magnetic resonance imaging (MRI) has a higher sensitivity than mammography for breast cancer detection [24-26]. Hence, the use of periodic breast screening with MRI in females at higher risk is recommended [27,28].

1.2.2 Diagnostic mammography

Diagnostic mammography is used to detect breast cancer in patients presenting with symptoms of this disease. These symptoms may include nipple discharge, a breast lump or breast skin color changes. Diagnostic mammography differs from screening mammography. Generally, during screening mammography only two views of each breast are obtained. However, diagnostic x-ray mammography includes multiple images or spot compression views to explore the positive finding in breast cancer patients [29]. Berg et al. showed that mammographic sensitivity for breast cancer varies from 34% to 81% depending on the cancer type [30], whereas Redmond et al. reported it to be 93.3% in detecting ductal carcinoma in situ (DCIS) [31]. Moreover, the sensitivity of the diagnostic mammography increases with the patient's age [32].

1.2.3 Diagnostic ultrasound

Ultrasonography is a non-invasive breast imaging tool that detects malignancy by bouncing sound waves off of breast tissue. An ultrasound transducer is used to receive acoustic waves reflected from the breast tissue to identify the internal structure of the breast. Ultrasound and x-ray mammography are complementary imaging modalities. Mammography is a key imaging modality for breast screening, but tumours may be occult to x-ray mammographic imaging in patients with dense breast tissue. Such tumours may be detected successfully using ultrasound imaging [33]. Diagnostic ultrasonography has significantly improved diagnostic accuracy and sensitivity for younger patients compared to x-ray mammography [31,34]. Thus, the combination of ultrasound and x-ray mammography can improve diagnostic accuracy of breast cancer.

1.2.4 Magnetic resonance imaging

Although x-ray mammography is widely available and acceptable, other imaging modalities have been intensively explored for breast imaging. MRI can play an important role in breast diagnosis, as it is a highly sensitive imaging modality. It has the ability to diagnose breast cancers that are occult on ultrasound and mammographic examinations [27]. Findings from MRI may alter the surgical strategy, such as a greater excision of breast tissue or choosing mastectomy [35]. The sensitivity of MRI for breast cancer detection varies from 89% to 96% according to the cancer type [30]. Additionally, MRI is more capable to detect multicentric breast cancer (more than one tumour, which are present in different quadrants of breast) compared to conventional x-ray mammography [36,37]. The presence of multicentricity is a contraindication for breast-conserving surgery (BCS). Hence, MRI findings along with other diagnostic images may assist the physician to make the decision of BCS or mastectomy.

1.3 Breast cancer surgery

The target of a cancer treatment is to remove the disease and to improve the quality of life of patient. Surgery is the main treatment option for breast cancer. Breast cancer surgeries differ from each other on the basis of the amount of tissue excised along with the tumour. The common types of surgical treatment include total mastectomy and BCS. Mastectomy is the complete removal of the breast, whereas BCS involves the removal of the cancerous tissue, along with a shell of healthy tissue enveloping the cancer to ensure the complete removal of the disease [38]. Radiation therapy following a BCS reduces the chance of local recurrence [39]. The type of surgery depends on the stage of breast cancer, size of the tumour, and patient consent. The surgeon discusses the advantages and disadvantages of the available options with the patient before making any decision.

1.4 Pathological evaluation of a surgery

The completeness of a BCS is assessed by pathological examination of the excised tissue. The goal is to determine the thickness of normal tissue between the surface of the specimen and the tumour. If the distance between the tumour and the edge of the excised specimen is ≥ 2 mm, then the tumour margin is considered as negative by most surgeons [40]. If cancer cells are present within a distance of 2 mm from the cut edge or exactly at the cut edge then the margin is

called a 'close margin' and a 'positive margin', respectively. In case of a close or positive margin, re-excision is performed depending on the surgeon's and patient's joint decision [40].

During the pathological evaluation, a pathologist takes a few slices from the surgically excised specimen, which are 3 mm to 10 mm apart [41]. Based on the examination of those slices the pathologist makes a decision of margin positivity. Although pathological evaluation is the gold standard for margin determination, it suffers from sparse sampling of the specimen. For example, evaluating a 2 cm diameter excised specimen by taking a 6 μ m thick slice through the greatest circumference, a pathologist examines less than 1% of the entire surface area of the excised cancerous specimen. In order to scrutinize the entire specimen more than 3000 slices are required, which is impractical. Additionally, this process will waste the entire specimen, which is required for additional histopathological testing [42]. Pathology reports are prepared approximately in two weeks and then the patient with a positive margin is recalled for a second surgery. The delay between the surgery and the news of a margin positivity is quite traumatic for patients. Thus, a technique is needed which can intra-operatively evaluate the tumour margin.

The presence of cancerous cells at the edge of the excised tissue (positive tumour margin) may increase the chance of local reoccurrence. A literature survey confirms that 6% to 55% of patients treated with BCS undergo a re-excision [43-45]. Re-excision results in poor cosmetic outcomes, increases healthcare costs, and psychological distress of the patient. The main reason for positive margins is the poor intra-operative image guidance for surgeons. The currently available techniques for this purpose are inadequate, and they are described in section 1.5.

1.5. Intra-operative guidance techniques

1.5.1 Palpation

If a tumour is palpable then the surgeon relies on palpation alone (no additional imaging is carried out), and the success of surgery depends on the experience of the surgeon and the preoperative imaging technique [46]. Physical examination under preoperative mammographic and ultrasound image guidance results in overestimation of tumour size, resulting in over excision. Moreover, lack of intra-operative image guidance leads the surgeon to be conservative in their approach removing excess tissue to ensure complete removal of the cancer. Furthermore,

palpation does not provide information of residual microscopic cancer in the surgical cavity [47]. To achieve clear margins, intra-operative palpation-guided surgeries result in large volumes of tissue being excised, which causes a deteriorating cosmetic outcome of the surgery. Krekel et al. reported that 98.8% excisions exceeded the optimal resection volume [46]. Additionally, palpation is not efficient of detecting occult and multicentric breast cancer. Young females have firm breast tissue which makes palpation inadequate to judge the tumour. Furthermore, surgeons face trouble in distinguishing between fibrotic tissue and the malignant breast mass through palpation [48].

1.5.2 Wire guided localization

Breast tumour detected in the early stage is nonpalpable, which necessitates the need for image guidance to localize such carcinomas [49]. Wire-guided localization (WGL) emerged as a solution for intra-operative guidance to remove nonpalpable breast tumours. WGL technique uses a wire to mark the position of the tumour to be excised. In breast cancer patients a guide wire is placed intratumorally under image guidance prior to surgery and this wire guides the excision of the cancerous tissue. Instead of a single wire, multiple wires can be placed to bracket a large area of calcification to reduce the volume of excised tissue, without affecting the margin status [50]. WGL is an effective technique for BCS and it is considered to be a gold standard procedure. However, it has been criticized because of a high percentage of patients with positive margins after WGL procedures. WGL ended up with a positive margin in 13.2% to 21.4% of patients [51-54]. Whereas, Ocal et al. observed only a 53% clear margin rate with WGL procedures [55]. The reason for a higher positive or close margin rate may be the lack of information about the three-dimensional position of the tumour, as the guide wire does not provide this information. Additionally, the wire placement is difficult in patients with dense breast tissue, and the migration of the wire may result in an excessive excision of the healthy tissue [55].

1.5.3 Intra-operative sonography (Ultrasound)

Currently, ultrasound is used as a tool for intra-operative guidance during BCS to excise non-palpable and palpable tumours. In intra-operative ultrasound (IOUS) procedures, the breast cancer patient is diagnosed with ultrasound preoperatively, and the tumour is localized during the surgery using the same ultrasound technique [56]. The percentage of patients with positive

tumour margin varies from 2.4% to 12.2% [52,57,58] in IOUS guided surgeries. Meta-analysis of ten different studies by Ahmed and Douek demonstrates that IOUS is advantageous over WGL to reduce the patient percentage with a positive margin [59]. Furthermore, Karanlik et al. compared ultrasound guided BCS to palpation-guided BCS and depicted that 17% re-excision in palpation-guided surgeries reduced to 6% in ultrasound-guided surgeries [60]. Additionally, the rate of poor cosmetic outcome after ultrasound-guided BCS dropped by 10% compared to palpation-guided surgeries [61]. In spite of improving cosmetic outcomes and reducing the positive margin cases, IOUS is not reliable to reveal the presence of DCIS. DCIS is characterized by calcification [62]. Breast carcinoma with microcalcification or spiculations extending beyond the tumour is difficult to visualize through ultrasound [62-64] because of ultrasound imaging artefacts. Moreover, it is difficult to detect microcalcifications with ultrasound when they are located inside echogenic and fibroglandular breast tissue, because it is hard to differentiate microcalcification from the echogenic interfaces among tissues [65]. Furthermore, surgeons require extensive training in ultrasound imaging for intra-operative applications, which is often not available. Thus, this technique may not be globally adapted.

1.5.4 Intra-operative radioactive seed localization

Radioactive Seed Localization (RSL) is an alternative to WGL to guide a surgeon intra-operatively and to improve BCS. Radioactive iodine-125 (3.7 to 10.7 MBq) embedded in a titanium seed is used in RSL guided surgeries. This radioactive material is a source of choice as it can be used in combination with technetium-99, which is used for the sentinel lymph node technique. Technetium-99 emits gamma rays of energy 140 keV, whereas ^{125}I emits gamma rays of energy 27 keV. Different peak energies of gamma rays make both radio-isotopes separately identifiable [66].

A radioactive iodine-125 (^{125}I) seed is placed in the cancerous breast through a needle, which is guided to the target location through mammography or ultrasound. The accuracy of the seed placement is confirmed through mammography. Due to a longer half-life of ^{125}I (60 days), a radioactive seed can be placed in the breast a few days prior to the surgery [66]. During the surgery a gamma-ray detection probe (GDP) is scanned over the breast to determine the focus of the highest activity to localize the radioactive seed. The region of intense activity is a target for the incision. The GDP also confirms the successful removal of the seed by scanning the wound

and the excised breast mass. Furthermore, radiographs of the excised specimen confirm the presence of the seed in it. During the pathological examination the radioactive seed is removed and sent to the nuclear medicine department in an appropriate shielding for decay before disposal [66].

The intra-operative RSL procedure has similar disadvantages to those of the WGL procedure. In RSL guided surgery, seed migration may result in an inadequate excision volume. Additionally, this technique does not provide any information about the presence of positive margins. Furthermore, RSL requires the additional training of surgeons and staff members in the operation theatre for the safe handling of radioactive seeds as the loss of a radioactive seed during a surgery has been reported in the literature [67].

1.5.5 Radio-guided surgery

The main target of radio-guided surgery (RGS) is to minimize the excision of the normal tissue along with the complete excision of a lesion. Conventional imaging techniques, such as x-ray mammography, ultrasound, and MRI, localize a tumour on the basis of its physical properties, such as dimensions and the position. However, nuclear medical imaging techniques differentiate healthy cells from malignant cells on the basis of their functional status. A tumour may possess an increased perfusion, an overexpression of cell surface receptors, and an expression of epitopes over the tumour surface. Anyone of these features can be radiolabeled to localize the cancerous tissue with the hand-held radiation detection probes, intra-operatively [68]. Currently, RGS includes radio-immuno guided surgery and beta particle guided surgery.

1.5.5.1 Radio-immuno guided surgery

Radio-immuno detection is a nuclear medicine imaging technique for the tumour localization. Radio-immuno guided surgery (RIGS) exploits overexpressed tumour associated antigens (TAA) for tumour delineation. A gamma rays emitting radiopharmaceutical (a monoclonal antibody tagged with a radioisotope) and a GDP, are components of a RIGS procedure.

A radiopharmaceutical is injected intravenously into the patient a few hours or days prior to the surgery. A monoclonal antibody specific to the TAA serves as the target vehicle for the radioisotope, which is conjugated to it. The monoclonal antibody attaches to the TAA along with a radionuclide, which increases the radioactivity at the binding site. The patient's body clears unwanted antibodies from the blood, which reduces the background activity. This

enhances the tumour-to-background (T:B) ratio, which is defined as the ratio of the radiopharmaceutical concentration present in the tumour to that of normal tissue. During surgery, a GDP is used to obtain a measure of radioactivity in the normal breast tissue by measuring the contralateral breast with the GDP. An activity higher than that of the activity in the normal tissue, represents the presence of cancer, which guides the surgeon for the removal of the tumour.

Breast cancer is characterized by the overexpression of TAA, such as tumour associated glycoprotein-72 (TAG-72), human epidermal growth factor receptor-2 (HER-2), human epidermal growth factor receptor-3 (HER-3), human carcinoembryonic antigen (CEA), which have been targeted by suitable radiopharmaceuticals [69-72]. TAG-72, HER-2, HER-3, and CEA, can be targeted with B72.3 monoclonal antibodies tagged with ^{111}In radioisotope [69], ^{111}I trastuzumab (Herceptin) fab [70], ^{111}I labelled NOTA conjugated antibodies [71], and anti-CEA antibody T84.66 labelled with ^{125}I radioisotope [72], respectively. Different studies including animals and human beings reported that a T:B ratio of 1.4 to 25.2 can be achieved by targeting different TAA with suitable monoclonal antibodies (Mabs) labeled with radio nuclides [69-71,73].

RIGS could be a solution for the breast tumour margin assessment. However, the Mabs are not only sensitive to the cancerous tissues; they also accumulate in distal organs and the proximal healthy tissue. Gamma rays emitted by a radionuclide have a long range in the tissue, and they can alter the GDP measurement significantly. Thus, the uptake of a radiopharmaceutical in distal organs may result in false positives. Additionally, the secretion of TAA from the tumour into the bloodstream may cause another problem for radio-immuno detection. The circulating antigens may bind to the Mabs to make an antigen-antibody complex, which decreases the quantity of radiopharmaceutical available for the tumour. Moreover, dehalogenation breaks the bond between radioactive iodine nuclides (^{111}I and ^{125}I) and antibodies at the tumour binding sites, which results in a higher concentration of radio isotopes in urinary excretion [74].

1.5.5.2 Beta particle guided surgery

The beta particle guided surgery is an alternative form of a nuclear medical imaging technique. A beta particle emitting radiopharmaceutical and a beta detecting probe are two components of a

beta guided surgery. A surgery of this type was performed for the first time in 1949. Patients with a brain tumour were injected with a beta particle emitter P^{32} , and a hand-held Geiger-Muller counter was used to guide the surgeon [75]. Since then, the radionuclide P^{32} has not been used for a long time, because it has a long half life, and it delivers a high radiation dose to the patient. Currently, several beta emitting radiopharmaceuticals are available. Table 2 represents different beta emitting radionuclides used in a clinic. Moreover, 2-Deoxy-2-[^{18}F] Fluoroglucose (^{18}F -FDG), a tracer for positron emission tomography, has been widely used to explore breast cancer [76-79]. It emits beta particles (positrons) with an end point energy of 633.5 keV.

Beta guided surgery takes advantage of the short range of a beta particle in the tissue. For example, a beta particle with maximum energy emitted by Fluorine-18 (^{18}F) has a continuous slow down approximation (CSDA) range of 2.4 mm in water. Thus, beta particles emitted by radiopharmaceutical present in distal organs will not increase the background signal due to the limited range of beta particles. This decreases the impact of the background radiation on the detector and improves the tumour detection. Additionally, the short range of the beta particle results in the improvement of the spatial sensitivity for the beta imagers compared to the gamma imager. Furthermore, the short range of the beta particle facilitates its absorption in a thin detector (of the order of mm) and eliminates the need of collimators, which leads to the construction of a compact detector to survey the surgical cavity. Moreover, developing a detector that can be placed a distance away from the patient and can examine the excised tumour reduces background photon detection originating from the radiopharmaceutical present in the patient. To date, few attempts have been made to develop imaging and non-imaging beta probes [80-88]. The detection sensitivity is the most important parameter of the probe to evaluate its performance. It depends on the radiation detection material, and the radiopharmaceutical [89]. Detection sensitivities of different beta probes have been discussed in section 1.7. In spite of higher detection sensitivity to evaluate surgical margins, beta detectors are unable to exploit deep seated tumours because of the short range of beta particles. However, gamma probes can detect cancer from a depth in soft tissue, because of less attenuation of gamma rays in tissue compared to beta particles.

Table 2. Characteristics of beta particle emitting radionuclides which are used or have the potential to be used in beta guided surgeries.

Radionuclide	Decay modes*	Half Life	Energy (keV)**	CSDA range ⁺ of beta in tissue (mm)
F-18	β^+	109.77 min	633.5	2.4
C-11	β^+	20.3 min	980	4.0
I-124	β^+	4.2 days	1535, 2138	7.3, 10.6
Ga-68	β^+	67.6 min	1899	9.3
Y-90	β^-	64 hours	2280	11.4
P-32	β^-	14.3 day	1710	8.3
I-131	β^-, γ	8.02 days	606.3, 364.5	2.3
Lu-177	β^-	6.7 days	498.3	1.5

* The decay modes with 15% or more probability are tabulated.

** End point energy of the beta particle spectrum.

⁺ Based on NIST database for electrons stopping power.

1.6 Definition of the problem

Beta detector-guided surgery has the potential to improve a BCS. Most importantly, a short range of beta particles in the tissue may result in reduced background noise and higher tumour-to-background radiation detection ratio. Thus, there is strong justification for studying and developing a single pixel beta particle sensitive detector.

1.6.1 Hypothesis

A beta detector can detect less than 1 mm² cancerous involvement on the surface of an excised tissue sample.

1.6.2 Specific objective

The objective of the thesis is to develop and evaluate a single pixel beta sensitive detector. The ultimate application of this detector is to detect the presence of cancerous cells at the surface of excised breast tissue.

In the present work, we are proposing an inorganic scintillation crystal optically coupled to a silicon photomultiplier (SiPM). A single pixel novel beta sensitive detector will be evaluated in this study.

1.7 Beta particle detection

Radiation detection with a detector/probe depends on the interaction of the incident radiation with the detector material.

1.7.1 Radiation interactions with absorber

Heavy charged particles (e.g., α particles) lose their energy through Coulomb interactions with the orbital electrons (collision losses) or the nuclei (radiation loss), within the absorber atom. The loss of energy through any interaction depends on traits of the absorber material and the incident particle. The energy loss of the charged particle per unit path length in a medium is called linear stopping power, which consists of two parts: 1. Radiation stopping power and 2. Collision stopping power.

Radiation stopping power is a result of the Coulomb interaction of the charged particle with the nucleus of an atom in the medium. The rate of the radiation loss is proportional to $(zZ/m)^2$, where z and m are the atomic number and the mass of the charged particle, respectively, and Z is the atomic number of the absorber. Light charged particles with high energy, lose significant energy through the radiation loss (bremsstrahlung radiation), whereas heavy charged particles lose negligible energy through this process compared to collision loss [90].

Collision stopping power is a result of the incident charged particle interaction with the orbital electron of the atom in the absorber. As a result of this event, the incident radiation transfers its energy to the electron, which may rise to higher energy states of the atom (excitation) or it may leave the atom (ionization). Both heavy and light charged particles lose significant energy through this process. Beta particles lose energy at a lower rate compared to

heavy charged particles and follow a tortuous path in the absorber. At low energies, collision loss is a major mechanism of energy loss of electrons and positrons. Positrons differ from electrons in terms of annihilation at the end of their range. The annihilation of a positron produces two gamma photons of energy 511 keV [90].

The photons produced during positron annihilation can further lose their energy within the detector. Gamma rays can interact with the detector material through photoelectric absorption, Compton scattering, and pair production. In the photoelectric absorption process a photon interacts with the bound electron of the absorber atom and completely loses its energy. The photoelectron produced during this process has an energy E_e given by

$$E_e = h\nu - E_b \quad (1.1)$$

where $h\nu$ is the energy of incident photon and E_b is the binding energy of the photoelectron in the original quantum state in the atom.

In Compton Scattering, the gamma photon interacts with the loosely bound electron of the atom, which recoils through an angle ϕ . During this event a photon transfers partial energy to the electron, and deviates through an angle θ from its original path. If E is the incident photon energy, the energy E' of scattered photon is given as

$$E' = \frac{E}{1 + \frac{E}{m_0 c^2} (1 - \cos \theta)} \quad (1.2)$$

where m_0 is the rest mass of electron and c is the velocity of light [90].

During the process of the pair production, an incident gamma photon of sufficient energy transforms into a pair of an electron and positron. This process takes place if the energy of gamma photon equals to or exceeds twice of the rest mass energy of an electron (1.02 MeV) [90].

Energy of the photons (511 keV) produced in positron annihilation is sufficiently less than the energy required to generate an event of pair production, and main mechanism of energy loss of such photons is photoelectric effect and Compton scattering. If Z is atomic number of the absorber, the probability of photoelectric absorption and Compton scattering per atom of the absorber is proportional to Z^5 and Z , respectively [90]. Thus, the detection material for gamma rays detector is chosen to have a high atomic number. However, the detection material in a beta

particle detector must be kept low to make the detector less sensitive to background gamma photons.

1.7.2 Beta particle detectors

Gamma-emitting radiopharmaceuticals emit gamma photons of a specific energy, whereas beta particles emitted by a radiopharmaceutical make a continuous energy spectrum. It necessitates the detection of the low energy as well as high energy beta particles, which can impact the sensitivity of the detector. Beta particle detection systems are of two types: 1. Direct detection, 2. Indirect detection.

1.7.2.1 Direct detection

A semiconductor detector directly converts the energy of an incident beta particle (or any ionizing radiation) to a measurable electrical signal. Incident radiation ionizes the semiconductor material of the detector and produces electron-hole pairs. The applied electric field exerts an electrostatic force on electrons and holes. They drift in opposite directions and are collected in corresponding electrodes, generating an electrical signal. This electrical signal is the measure of energy deposited by the incident particle in the detector.

In an ideal semiconductor, charge carriers produced in an ionization event must reach their respective electrodes. However, the impurities in the realistic semiconductor material trap a charge carrier for a long time, which prevents it from contributing to the detector signal. Additionally, impurities may trap both an electron and a hole, causing them to recombine, which reduces the charge collected at the electrodes. Moreover, semiconductor detectors show certain conductivity without any interaction with the ionizing radiation, which results in a leakage current. The leakage current is a significant source of noise, and techniques of lowering the leakage current are always required while designing semiconductor detectors [91].

Different research groups have developed silicon-based pixelated semiconductor beta detectors with a pixel size of approximately $1 \times 1 \text{ mm}^2$ [81,83] for intra-operative guidance. The detection sensitivity of the pixelated detector developed by Huh et al. [83] was less than 4 CPS/kBq, and Tornai et al. [81] obtained a beta to gamma detection ratio of approximately 40. However, semiconductor detectors are highly sensitive to temperature variations and require cooling to work consistently.

1.7.2.2 Indirect detection

Another effort in developing beta probes involves indirect detection using a scintillation material. An ionizing radiation enters the scintillation material, loses its energy, and excites the electrons of the scintillation material to higher energy states. During the subsequent de-excitation, the scintillator produces light photons in the visible region. The number of photons produced is proportional to the energy deposited by the incident radiation in the scintillator. The scintillation light is further transported to a photodetector through direct coupling or through optical fibers. Scintillation light photons ionize the detection material of the photodetector. Electrons produced in these events are multiplied and then collected at the anode of the photodetector to produce an electrical signal. The electrical signal produced by the photodetector, indirectly provides a measure of the energy of the incident radiation. Scintillators and photodetectors are further described in sections 1.7.3 and 1.7.4, respectively.

1.7.3 Scintillator

An ideal scintillator for the application of a beta detector should absorb an incident radiation completely, and convert its energy to detectable light photons (i.e., it should provide high scintillation efficiency). High scintillation efficiency causes high scintillation light output, which can lead to detection of low energy radiation. The light produced in a scintillator should be proportional to the energy of an incident particle, which could be helpful to resolve the energy of incident radiation. Additionally, the decay time of a scintillator needs to be short and its refractive index should be comparable to that of glass, to permit an efficient coupling of the scintillator to the photodetector. Moreover, scintillator should be transparent to scintillation light which results in the maximum light yield from the scintillator [91].

There is no ideal scintillation material that has all the properties mentioned above. The choice of a scintillator is always a compromise between these properties. Inorganic and organic materials are most widely used as a scintillator in a radiation detector. Inorganic scintillators are known to have a superior light output, but they have a longer decay time. However, organic scintillators are faster in response with a low light yield. Additionally, a scintillator with a high effective atomic number is appropriate for gamma ray detection [91]. However, a scintillation material with a low effective atomic number is less sensitive to gamma photons and suitable for

beta particle detection in the presence of gamma background radiation. Table 3 represents properties of scintillators suitable for beta particle detection [92].

Table 3. Properties of organic and inorganic scintillators suitable for beta particles detection.

Characteristic	BC400	Anthracene	BC404	CaF ₂ (Eu)
Type	Organic	Organic	Organic	Inorganic
Effective Z	5.67	5.7	5.76	16.9
Density (g/cm ³)	1.032	1.25	1.032	3.18
Light Output (k ph/Mev)	10.7	16.5	11.2	24
Attenuation Length (cm)	250	-----	160	2-5
Peak wavelength of emission (nm)	423	447	408	424
Decay constant (ns)	2.4	30	1.8	940
Refractive Index	1.58	1.62	1.58	1.44
Hygroscopic	No	No	No	No

Among all crystals suitable for beta detection, CaF₂(Eu) produces high scintillation light. Moreover, CaF₂(Eu) has higher atomic number compared to organic scintillators, which permits to use a thin scintillator to minimize background gamma ray detection without affecting beta detection sensitivity. Gamma photons are highly penetrating radiation and they can reach the detector even if they are produced deeper in the tissue. The reduced gamma ray (background radiation) detection sensitivity of the detector can improve the tumour-to-background radiation detection ratio, which leads to the detection of small deposits of cancer cells.

1.7.4 Photodetector

A photodetector collects the light emitted by a scintillator coupled to it, and converts it to a measurable electrical signal. This signal is proportional to the energy deposited by the light photons in the photodetector. A photomultiplier tube (PMT) and a silicon photomultiplier are two common types of photodetectors.

1.7.4.1 Photomultiplier tube

A photomultiplier tube is widely used as a photodetector in a scintillation detection system. It consists of a vacuum tube, which houses a photocathode, multistage dynodes (electron multiplier structure), and an anode. The photocathode absorbs light photons and then emits low energy electrons. A few number of electrons are produced, which cannot serve as an electrical signal. The electron multiplier structure amplifies the number of electrons originally produced at the photocathode. After an amplification, a scintillation event results in 10^7 - 10^{10} electrons. These electrons are collected at the anode to produce a measurable electrical signal [91].

1.7.4.2 Semiconductor photodetector

There are mainly three types of semiconductor photodetectors: a photodiode, an avalanche photodiode (APD), and a SiPM. A photodiode is a p-n junction or a PIN semiconductor detector designed to operate in a reverse bias condition. Optical photons of sufficient energy (greater than the band gap of the semiconductor material) fall on the device in the depletion region and lose their energy to produce electron-hole pairs. The built-in electric field of the depletion region sweeps these charge carriers from the junction. The holes move towards the anode and the electrons towards the cathode, which results in a photocurrent proportional to the number of incident photons. A photodiode is suitable for an application where a compact detector design is required. However, the use of a photodiode is limited because of their low internal gain, which is of the order of unity.

The physics behind the functioning of an APD is the same as that of a simple photodiode, except an APD works at a high reverse bias voltage. This voltage is less than the breakdown voltage of the APD, but it is sufficient to generate impact ionization. During impact ionization the electrons created by incident photon in the depletion region gains sufficient energy from the applied field and collide with an electron in valance band of the radiation detection material to excite it to the conduction band. In this way additional electron-hole pairs

are produced. The electrons produced during this process drift towards the anode and the holes drift towards the cathode, to generate an amplified signal proportional to the number of incident photons. APD gain is limited by applied reverse bias voltage and impact ionization in an APD leads to an internal gain of the order of 100, with a bias voltage of 100-200V. With an applied voltage higher than 1500V, a gain of several thousand electrons is possible with a specially manufactured APD, which is much less compared to a PMT [93].

The gain of an APD can be improved by making them to work in a Geiger Mode. If an APD works with a reverse bias voltage above the breakdown voltage, it is termed as a Geiger Mode APD (GM-APD). Contrary to an APD, in a GM-APD, electrons generated during the impact ionization are accelerated by the applied voltage, and are further used in an avalanche process. In this way, a gain of the order of 10^6 is achieved, which is comparable to a PMT. However, a GM-APD has the limitation that its output signal is the same for any number of input photons.

A SiPM overcomes the lack of proportionality of the GM-APD output. A SiPM consists of an array of 100-1000, GM-APDs connected in parallel. Each GM-APD is called a micro-cell and produces an electrical signal when a photon activates it. Each individual micro-cell detects photons independently and the output signal of a SiPM is directly proportional to the number of microcells activated by photons. A SiPM offers several advantages over a conventional PMT. They have a compact and robust structure, which is insensitive to a magnetic field. Thus, a compact scintillator detector can be designed, by optically coupling a SiPM to a scintillator, which can work in the magnetic field environment. Additionally, a SiPM has a low operating voltage, which is of the order of 30V and it is efficient for the detection of a low light signal of the order of a single photon. The light detection efficiency of a SiPM (sensl, C-series 30035, Cork, Ireland) is more than 40% [94]. This makes the SiPM able to detect low light signals produced by low energy radiation in the scintillator coupled to it.

1.7.5 Existing beta scintillation detectors

Daghighian et al. made a beta probe consisting of two separate plastic scintillators, where one of them was shielded from beta particle [80]. After subtracting the signals from each of the scintillators, a beta particle signal was isolated. Weighted subtraction of gamma counts from counts detected by the first scintillator gives the number of beta particles detected by the first

detector. The beta particle detection sensitivity of this method was reported as being 108 CPS/kBq with ^{18}F . An alternate method was proposed by Yamamoto et al. to construct a phoswich beta detector. This detector consisted of the combination of a plastic scintillator and a bismuth germanate (BGO) scintillator placed in apposition [82]. The plastic scintillator in the front position detects a positron, and is coupled with the BGO scintillator, which detects a gamma photon produced by the annihilating beta particle in the plastic scintillator. Thus, the detector counts coincident events (beta particle and one of the corresponding annihilation photons) and suppresses accompanying spurious background gamma photons. If any background photon loses its energy in the plastic scintillator or in the BGO crystal alone, such events are not registered by the pulse shaping circuit. The reported detection sensitivity of the phoswich detector is 2.6 CPS/kBq. Here, the gamma rejection is achieved at the cost of a loss of beta particle sensitivity. Additionally, in above mentioned beta probes, a scintillator is coupled with a PMT through an optical fiber. Coupling with optical fiber is done to keep the detector dimensions small, and to provide electrical insulation to a PMT from the patient's body [95]. However, optical fibers are always associated with a light loss due to absorption, scattering of light photons, and bending losses. Cherry et al. experimentally found that a scintillator coupled with a PMT, through an optical fiber, transmitted 23% of the signal obtained by direct coupling of the detector components [96]. In another study, Tornai et al. coupled a scintillator to a PMT through an optical fibre and registered 33% loss in pulse height compared to direct coupling [97].

Scintillation light collection and beta particle detection sensitivity can be improved by using a SiPM as a photodetector. It has a superior light detection efficiency compared to a PMT. Additionally, it can be directly coupled with a scintillator allowing a compact probe/detector structure. Moreover, a SiPM has a low voltage operating characteristic, which eliminates the risk associated with a PMT because of a high operating voltage. Furthermore, a SiPM can operate at the room temperature and no warm up time is required. In the last few years several beta particle probes have been developed to reap the benefits of the SiPM technology [84-86,88].

1.8 Newly proposed beta detector and its characterization

Based on existing techniques of developing beta probes, a new design of a single pixel prototype intra-operative beta particle detector has been proposed in this thesis. The detector prototype

consists of a $3 \times 3 \text{ mm}^2$, $\text{CaF}_2(\text{Eu})$ scintillation crystal, optically coupled to a SiPM. The $\text{CaF}_2(\text{Eu})$ scintillator has high light yield and light transport efficiency. These properties of the scintillator make it suitable to detect low energy beta particles. Beta particles that originate from deeply seated tumours (on the order of millimetres) have low energies. Thus, $\text{CaF}_2(\text{Eu})$ scintillation detector can be used to reveal the presence of cancer cells up to a depth of few millimetres. Additionally, its low effective atomic number and density make it less sensitive to spurious gamma photons.

In the present study, a SiPM is used as a photodetector, and it is directly coupled to a $\text{CaF}_2(\text{Eu})$ scintillation crystal. The $\text{CaF}_2(\text{Eu})$ scintillator has a peak emission wavelength of 435 nm, whereas the light detection efficiency of a SiPM (sensl, C-series 30035, Cork, Ireland) is approximately 40% at this wavelength [94]. Additionally, direct coupling results in better light collection at the SiPM. Moreover, the small size of SiPM preserves the compactness of the detector. The high light yield of $\text{CaF}_2(\text{Eu})$ and high light collection of a SiPM may result in a better detection efficiency of the detector compared to detectors based on organic scintillators.

Finally, an *in silico* study is used for detector characterization to reveal the presence of malignancy at the cut edge of the surgically excised breast tissue. Surveying the excised tissue away from the patient potentially reduces the impact of the spurious background radiation. This facilitates the detection of cancer deposits that are less than 1 mm^2 at the cut edge of the excised tissue. Cancer cells at the surface of the excised tissue are directly linked with the remnant disease in the surgical cavity, which can be re-excised during the surgery.

The newly designed beta detector is a single pixel prototype of a large area scanner ($10 \times 10 \text{ cm}^2$), which could evaluate the entire surface of the surgically excised cancerous breast tissue during BCS.

1.9 Thesis overview

Chapter 2 describes the construction of a single pixel beta sensitive detector, the method, and results, of the $\text{CaF}_2(\text{Eu})$ crystal thickness optimization for the superior beta to gamma detection ratio. Chapter 2 also describes the method and results of the detector characterization to determine a minimum detectable tumour surface area at the cut edge of the surgically excised tumour model. A complete overview of the thesis, discussion of overall findings and future work are included in Chapter 3.

Chapter 2 Construction and characterization of a novel single pixel beta detector for intra-operative guidance in breast-conserving surgery

This chapter represents an under-review manuscript: "Amritpal Singh, John Dillon, Ananth Ravi. Characterization of a single pixel beta detector for guidance in breast-conserving surgery" submitted to the Transactions on Radiation and Plasma Medical Sciences. Amritpal Singh was responsible for collection and administration of the research studies, data analysis and writing the manuscript.

2.1 Abstract

Breast-conserving surgery (BCS) is the primary treatment option for early stage breast cancers. It is a challenging surgical procedure due to the lack of intra-operative guidance methods available to surgeons. One potential method of guidance would be to leverage radiopharmaceuticals used in the clinical work-up of breast cancer for intra-operative guidance. Patients could be injected with radiopharmaceuticals that emit beta particles and preferentially accumulate within cancer cells. Then at the time of the surgery, a beta particle detector could be used to intra-operatively guide the complete excision of the tumour. Detection of beta particles enables the surface interrogation of the sample/cavity without being confounded by accumulations of the radiopharmaceutical at depth. The purpose of this study is to develop and analyze a novel single pixel beta sensitive detector, which would be capable of intra-operative margin evaluation of the entire specimen. **Method:-** The single pixel detector is made up of a calcium fluoride europium doped scintillation crystal, $\text{CaF}_2(\text{Eu})$, optically coupled to a silicon photomultiplier (SiPM). $\text{CaF}_2(\text{Eu})$ was selected for its beta sensitivity, gamma insensitivity, and light yield. Silicon photomultiplier was selected as a photon detector because of its robustness, small form-factor, and low operating voltage compared to a conventional photomultiplier tube (PMT). The scintillation crystal thickness was optimized prior to the characterization of the system as a whole. The optimized crystal thickness was used to assemble a novel single pixel beta sensitive detector by optically coupling it with a SiPM. A computational model of the detector response was derived from an empirically generated, two-dimensional (2D), sensitivity map of the beta detector. Using this computational model, the study tested whether the novel detector could detect, with a sensitivity and specificity of 95%, involvement of the margin using simulated clinically realistic excised cancerous breast tissue during a BCS. **Results:-** The overall detection sensitivity of 0.5 mm, 1.0 mm, and 1.5 mm thick $\text{CaF}_2(\text{Eu})$ crystals was 19 ± 2 , 22 ± 3 , and 24 ± 3 CPS/kBq, respectively while beta to gamma detection ratio for the similar settings

was 8.1 ± 0.7 , 4.9 ± 0.3 , and 3.6 ± 0.4 , respectively. A crystal thickness of 0.5 mm was selected as the scintillating element of the detector as this scintillator provided similar beta counts to the other thicknesses with significantly improved gamma rejection. A clinically realistic tumour model was developed to determine the minimum detectable tumour surface area of margin involvement as a function of acquisition time, tumour-to-background (T:B) ratio, and normal tissue background activity. According to this study, it is expected that with an acquisition time of 30 seconds, the T:B ratio of 5 or higher, and a normal breast tissue activity of 1.69 kBq/ml, less than 1 mm² tumour detection is feasible. Results of this study indicate that radio-guided surgery with a CaF₂(Eu) scintillation detector could be feasible to intra-operatively assess tumour margin involvement.

2.2 Introduction

In North America more than 60% of breast cancer patients undergo breast-conserving surgery (BCS) [38,98]. This surgery involves the excision of cancerous tissue along with a shell of healthy tissue [38]. During BCS, healthy tissue is excised in order to ensure the removal of the microscopic disease close to tumour edges. Two challenging goals of this operative procedure are to remove the whole disease and minimize the volume of healthy tissue removed to improve cosmetic outcomes.

Presently, only limited intra-operative guidance strategies are available to surgeons. Feasible palpation is used to delineate tumour edges, but this technique is challenging when distinguishing between fibrotic tissue and a tumour. On the other hand, wire-guided localization (WGL) is utilized for intra-operative guidance to remove tumours which cannot be palpated. This technique has been widely criticized, as it does not provide any information about tumour boundaries, and results in up to 47% close margin and positive margin rates [51-55,99]. Radioactive seed localization (RSL) is an alternative to WGL; however, this technique localizes the center of the lesion without providing any information about tumour margins. According to a meta-analysis, positive and close tumour margin rates range from 3% to 30.3% in RSL guided surgeries [100].

Alternatively, nuclear medicine imaging techniques distinguish cancer cells from normal cells on the basis of their functional status, which can determine whether gross margins are clear intra-operatively. Influenced by the potential of this technique, researchers explored radio-

immuno guided surgery (RIGS) to improve BCS. RIGS uses a gamma emitting radiopharmaceutical to target cancer cells and a gamma-ray detection probe for the surgical guidance. Since gamma rays are highly penetrating, RIGS suffers from a high level of background radiation due to the nonspecific uptake of the radiopharmaceutical [101].

Beta particle guided surgeries have the potential to overcome the problem caused by background radiation in RIGS. The range of beta particles emitted by clinically available radiopharmaceuticals is of the order of millimetres in water [92]. As such, radiopharmaceuticals present in distal organs because of non-specific uptake will not inadvertently increase the background signal due to the limited range of beta particles. Hence, beta particles could provide a high tumour-to-background radiation detection ratio, which is defined as the ratio of radiation counts detected from the tumour to counts detected from background tissue. Thus, a smaller minimum detectable margin involvement can be achieved. Previous approaches to build beta sensitive probes to examine the surgical cavity/excised cancerous tissue are listed in Table 4.

Table 4. Beta particle sensitive probes/detectors

Probe developer	Beta particle detection	Radiation detection elements	Background gamma noise rejection	Sensitivity (CPS/kBq)	Field of View (mm ²)
Daghighian et al., 1994	Indirect	Two concentric Pl. Sci. + PMTs	Subtraction	108 (Contact)	~ 125
Yamamoto et al., 2005	Indirect	Pl. Sci. + BGO Sci. + PMT	Coincidence	2.6 (with a 5 mm collimator)	~ 218
Spadola et al. 2016	Indirect	P-Ter. + SiPM	-----	321 (Contact)	~ 660
Camillocci et al., 2017	Indirect	P-Ter. + SiPM	-----	-----	~ 20
Tornai et al., 2002	Direct	Silicon	-----	-----	256

Abbreviations: Pl. = Plastic, Sci. = Scintillator, and P-Ter. = Para-Terphenyl

In the present study, we are building upon past efforts to create a sensitive beta detector to develop a novel single pixel prototype detector. The prototype detector is designed in such a way that the $\text{CaF}_2(\text{Eu})$ scintillation crystal is directly coupled to a silicon photomultiplier (SiPM), therefore resulting in a compact detector structure. Moreover, this feasibility study evaluates whether a novel beta particle detector can detect $< 1\text{mm}^2$ deposits of cancer cells at the cut edge of surgically excised breast tissue, under clinically relevant conditions.

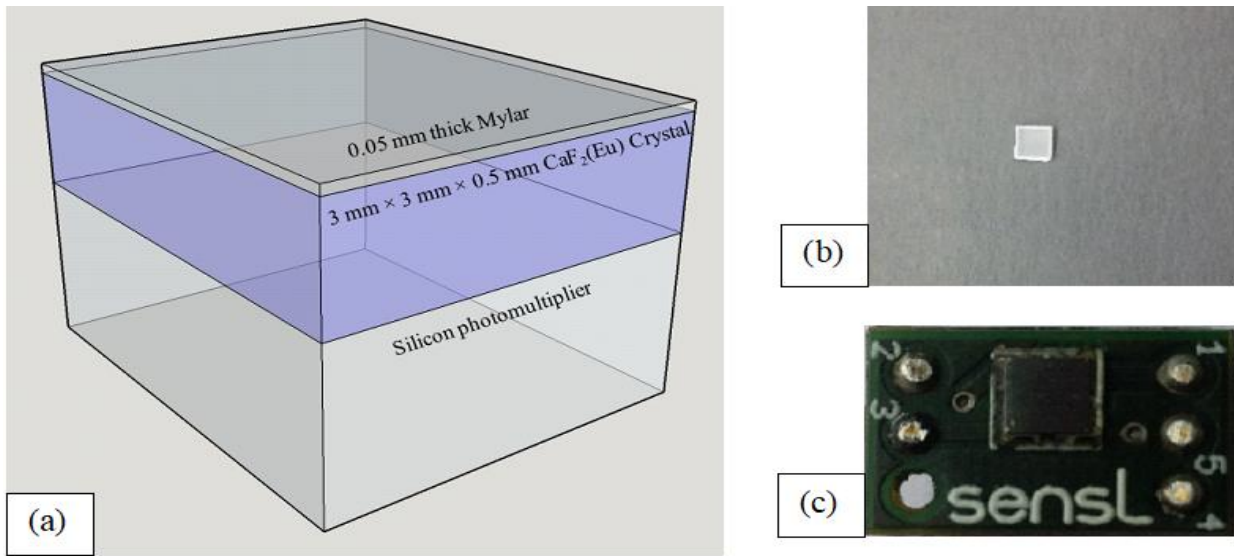
2.3 Methods

2.3.1 Beta particle detector

The intra-operative beta sensitive detector consisted of a $\text{CaF}_2(\text{Eu})$ scintillation crystal optically coupled with a silicon photomultiplier (SiPM) (sensl, C-series 30035, Cork, Ireland). An optical gel (Cargille Optical Gel with an index of refraction of 1.46) was used for this purpose. A $\text{CaF}_2(\text{Eu})$ scintillator has a light production efficiency of more than 24000 photons/MeV [102] [103]. The direct coupling of the scintillation crystal with a SiPM eliminates the use of optical fibres, which minimizes the loss of scintillation light photons. Moreover, room-temperature operation of the crystal does not impair its light production efficiency, eliminating the requirement of crystal cooling.

The scintillation crystal thickness was optimized to obtain a superior beta particle detection sensitivity compared to gamma ray photons. The $\text{CaF}_2(\text{Eu})$ scintillation crystal measured $3 \times 3 \text{ mm}^2$. The assembled detector was encased in polyformaldehyde, which was lined with a copper sheet in order to provide electromagnetic shielding. The detector case had an opening window, which was covered with 0.05 mm thick Mylar.

The amplification, pulse shaping, and pulse discrimination, were carried out by a delay line amplifier (ORTEC 460) (Figure 4 b). The amplified and shaped output signal was input into a multichannel analyzer (ORTEC EASY-MCA) connected to a personal computer.



Schematic diagram of the single pixel beta sensitive detector where a silicon photomultiplier is directly coupled to the scintillation crystal. Photographs of detector components (b) CaF₂(Eu) crystal (c) sensl 30035 SiPM

Figure 2. Structure of the beta sensitive single pixel detector.

2.3.2 Crystal thickness optimization

The CaF₂(Eu) crystal thickness varied to optimize the beta to gamma detection ratio. Three crystals with different thicknesses (0.5 mm, 1.0 mm and 1.5 mm) were evaluated.

The radioactive source was made up of Polymethyl Methacrylate (PMMA) with 10 mm diameter and 2 mm height (Figure 3). A cylindrical cavity of 2 mm diameter and 1.9 mm length was machined in PMMA and this cavity was filled with beta particles (positrons) emitting radiopharmaceutical; 2-Deoxy-2-[¹⁸F] Fluoroglucose (¹⁸F-FDG) having an activity of 13.7 ± 0.2 MBq. The source cavity was designed to have a similar diameter as that of milk ducts in a breast, which varies from 1.2 - 2.5 mm [104].

Each crystal thickness was evaluated by placing the ¹⁸F-FDG source, at 1.13 mm from the detector surface. This separation was sufficient to insert a beta shielding material between the source and the detector. A combined spectrum of beta and gamma radiation was obtained at this distance. Subsequently, a gamma spectrum was measured by blocking beta particles with a copper sheet of thickness 0.56 mm. This thickness was used because the continuous slow down approximation (CSDA) range of the maximum energy (633.5 keV) beta particle emitted by ¹⁸F

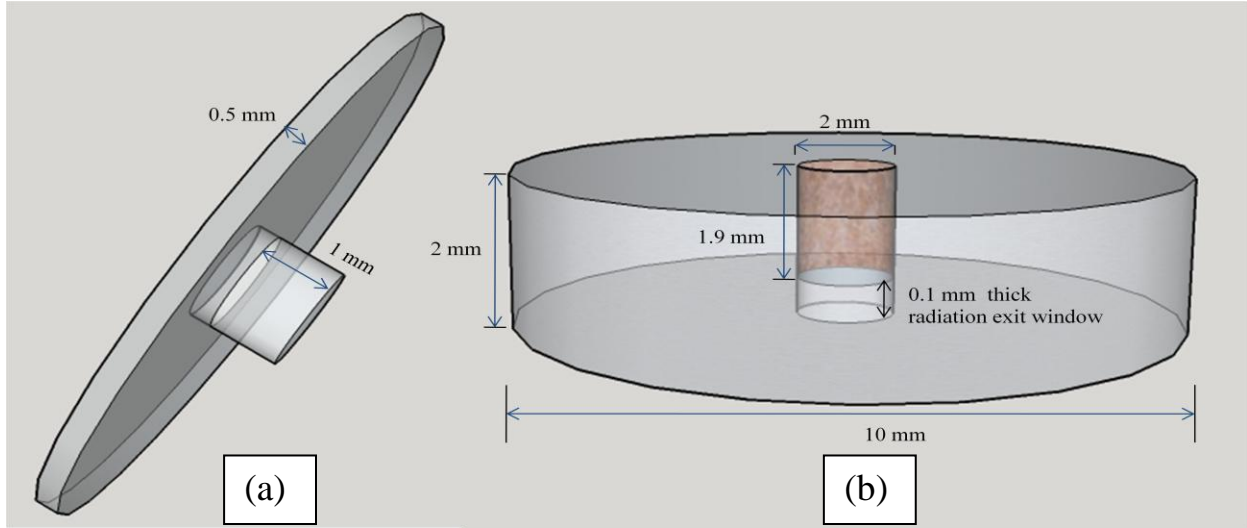


Figure 3. Schematic diagram of source geometry. (a) Lid of the ^{18}F -FDG vial. (b) Vial with 2 mm diameter to house ^{18}F -FDG.

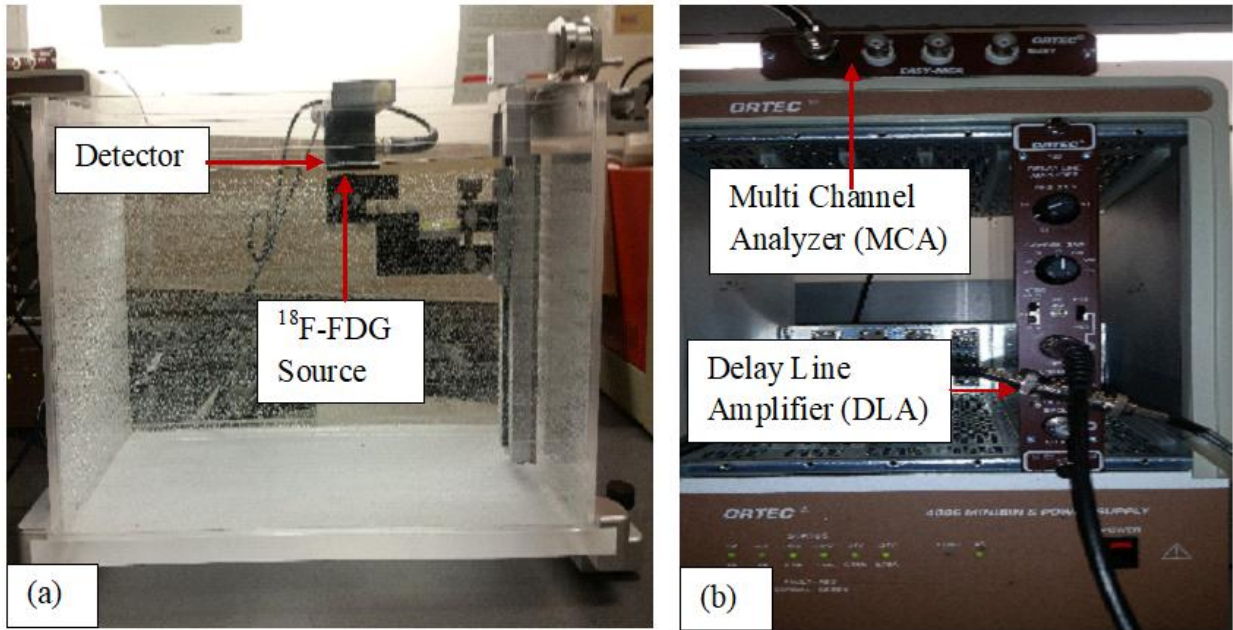
is 0.40 mm in copper [105]. Thus, 0.56 mm thick copper is sufficient to block a maximum number of beta particles, as well as bremsstrahlung radiation produced in the copper sheet. In addition to the beta particle shielding, the copper sheet also attenuates photons passing through it. Thus, the true photon spectrum was obtained after the correction for the photon attenuation to the measured photon spectrum. The true photon spectrum was subtracted from the combined spectrum, which yielded the beta particle spectrum. The data collection was repeated six times for each of the three detectors.

2.3.3 Creating a detector sensitivity map

The sensitivity map of the prototype detector, with an optimized scintillation crystal thickness, was created. The detector was mounted facing a radioactive source in a water tank (Figure 4 a). Water tank was used to acquire the sensitivity map in order to incorporate the attenuation of photons and beta particles as expected in breast tissue. The two-dimensional (2D) detector sensitivity map was acquired with the radioactive source described above in section 2.3.2. The source was translated away from the detector (axially) and parallel to the detector (horizontally) in the water tank, to generate 171 measurements in 2D space. An area of $10 \times 10 \text{ cm}^2$ was measured and was subdivided into three different regions. In the detector vicinity of $1 \times 1 \text{ cm}^2$, measurements were taken with 1% relative error and a fine resolution of 1 mm as the sensitivity

changes rapidly. The data was recorded with a coarser resolution of 10 mm up to $5 \times 5 \text{ cm}^2$ and 25 mm up to $10 \times 10 \text{ cm}^2$ with a 5% relative error.

The experiment was repeated five times to obtain 2D detector sensitivity map. The three-dimensional (3D) detector sensitivity map was obtained by rotating the 2D detector sensitivity map around the central axis of rotational symmetry of the detector. A similar approach was adopted by Ravi et al. to create a sensitivity map of a gamma-ray detecting probe [101].



Source facing the detector placed in the water tank. The source is movable in the horizontal and the vertical direction.

The detector output is fed to a DLA and then to a MCA to generate energy spectrum of the source at different positions.

Figure 4. Apparatus used to acquire the sensitivity map of the beta sensitive detector for ^{18}F -FDG radiopharmaceutical.

2.3.4 Minimum detectable tumour surface area (MDTSA)

Presently, the re-excision rate vary from approximately 6% to 55% [43-45], which can be considered as a measure of false negative rates associated with BCS. If the beta particle guided surgeries can lower this re-excision rate, this would be beneficial for breast cancer patients. Therefore, a 5% false negative and a 5 % false positive rate was set as a detection goal to improve the quality of BCS. Based on Currie's criteria, to obtain a 5% false positive a critical limit of detection L_C was defined by the following equation [106]:

$$L_C = 2.326\sqrt{\mu_B} \quad (2.1)$$

L_C sets a level of measurement, in the presence of background counts μ_B , above which an error is made if it is assumed that there is no detection. Similarly, a detection limit defines a level of measurement below which an error is made if it is stated that there is a detection. To achieve a 5% false negative rate, a detection limit was obtained as follows [106]:

$$L_D = 2.71 + 4.65\sqrt{\mu_B} \quad (2.2)$$

L_D is the least number of counts detected by the detector to confirm the existence of cancer cells at the cut edge of the surgically removed tissue in the presence of background counts μ_B . The source of background radiation in the excised tissue is the radiopharmaceutical present in the macroscopic tumour and the surrounding healthy tissue.

A phantom was created by modeling a surgically excised cancerous breast tissue using MATLAB (MATLAB 9.2, MathWorks, Inc., Natick, MA, US). The model consisted of an ellipsoidal tumour having semi-axes (1.5 cm, 1.5 cm, 1.0 cm) enveloped with 1 cm thick normal breast tissue (Figure 5 a) to mimic the clinical scenario. Each voxel in the simulated excised tissue was labelled as healthy tissue or cancerous tissue and was populated with the appropriate ^{18}F -FGD activity (in kBq). Multiplication of the activity of each voxel with the detector sensitivity (in CPS/kBq) at the voxel location provides counts per second detected by the detector from a specific voxel. Overall counts detected by the detector from all voxels represent the background counts detected by the detector.

Iterative tumour growth (from the macroscopic tumour boundary to the cut edge of the excised tissue) was simulated in the steps of $1 \times 1 \times 10 \text{ mm}^3$ cuboids (Figure 5 b) and the expected counts were calculated after each iteration. When the simulated counts detected by the detector were greater than or equal to the detection limit L_D , iterations were stopped and the surface area of the tumour at the cut edge of the excised tissue was calculated. This surface area of the tumour represents the minimum detectable tumour surface area (MDTSA). L_D is a function of background activity, which is related to the variation in normal breast tissue uptake of the radiopharmaceutical. Radiopharmaceutical uptake in breast tissue was approximated from reported standardized uptake values (SUV) for breast tissue in the literature. SUV is defined as follows [107]:

$$SUV = \frac{mCi/ml \text{ (decay - corrected) in tissue}}{mCi \text{ of radiopharmaceutical injected} / \text{patient body weight (g)}} \quad (2.3)$$

The average standardized uptake value (SUV_{avg}) of ^{18}F -FDG within normal breast tissue varies from 0.20 to 1.30 [108-110] with a median value of 0.50 [108]. The mean value of maximum standardized uptake value (SUV_{max}) in breast tumours varies from 2.9 to 4.8 [111-114] in patients who may be eligible for BCS.

With the normal tissue activity derived from the SUV data to be 1.69 kBq/ml and the tumour-to-background (T:B) ratio fixed at 7, MDTSA was characterized as a function of acquisition time. Keeping the acquisition time fixed at 30 seconds and the T:B ratio fixed at 7, MDTSA was also characterized as a function of the normal tissue activity. Lastly, MDTSA was characterized as a function of T:B ratio with the acquisition time specified at 30 seconds and the healthy tissue activity specified at 1.69 kBq/ml.

Table 5. Average SUV (SUV_{avg}), mean, and median SUV_{avg} , in normal breast tissue for patients with different breast density and menopausal status.

Research Group	Range of SUV_{avg}	Mean SUV_{avg}	Median SUV_{avg}	Patients included in the study
Zytoon et al. 2013 [108]	0.20-1.30	0.52 ± 0.23	0.50	Women with different menopausal status
Kumar et al. 2006 [109]	0.60-0.77	Dense breast 0.84 ± 0.27 Nondense breast 0.53 ± 0.23	-----	Women with different breast density and menopausal status
Vranjesevic et al. 2003 [110]	0.22-0.39	Right dense breast 0.39 ± 0.05 Left dense breast 0.36 ± 0.07	-----	Women with different breast density and menopausal status

Table 6. Maximum SUV (SUV_{max}), mean, and median SUV_{max} in breast tumours for patients who may be eligible for a BCS.

Research group	Range of SUV_{max}	Mean SUV_{max}	Median SUV_{max}	Patients included in the study
Azuma et al. 2008 [112]	2.2-3.4	2.9		Patients with pure DCIS
Basu et al. 2008 [111]	-----	2.9 ± 2.7		Patients without any metastasis
Koolen et al. 2014 [114]	-----	-----	3.5	Patients with IDC
Tateishi et al. 2012 [113]	-----	4.4 ± 3.1		Patients with tumour size 1.8 to 12 cm
Basu et al. 2008 [111]	-----	4.8 ± 3.9		Patients with primary breast cancer and metastatic axillary lymphadenopathy

Abbreviation IDC = Invasive ductal carcinoma

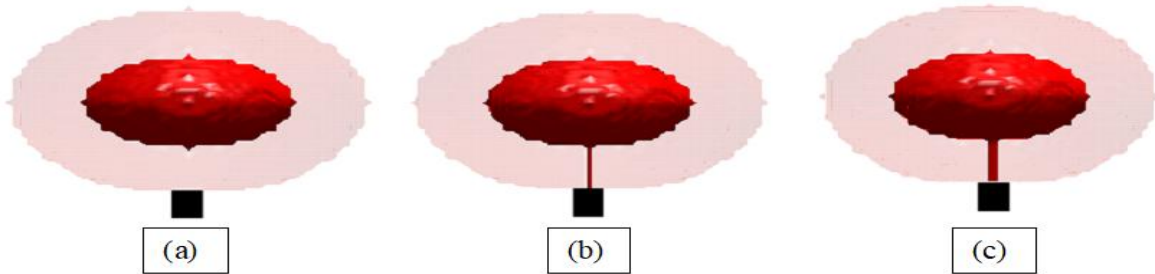


Figure 5. Pictorial representation of the modeled surgically excised tumour and its iterative growth in the breast duct used to determine MDTSA at the cut edge of the excised breast tissue. Dark red and light red colors in the above figures represent tumour cells and healthy tissue surrounding the tumour in the excised breast mass, respectively. (a) Modeled ellipsoidal tumour with semi-axes 1.5 cm, 1.5 cm, 1 cm within a shell of 1 cm healthy breast tissue. (b) The dark red column is the first step of tumour growth with dimensions of $1 \times 1 \times 10 \text{ mm}^3$ (c) Next step of iteration with an additional column of $1 \times 1 \times 10 \text{ mm}^3$ tumour cells.

Figures 5(b) and 5(c) represent the tumour growth pattern used in the algorithm, which demonstrates the worst case scenario of the tumour growth as the minimum cancer cells are in the closest neighborhood of the detector.

2.4 Results

2.4.1 Crystal thickness optimization

Figures 6(a), 6(b), and 6(c) represent overall spectra, photon spectra, and beta spectra, respectively of the ^{18}F -FDG source. Each of the three plots is an average of six measurements and error bars were generated by accounting for the standard deviation in measurements. The large standard deviation in measurements is expected because of the uncertainty in the activity of different ^{18}F -FDG sources. The combined (photons + betas), photon, and beta detection sensitivities, of the three beta detectors, are represented in Table 7. All measurements were obtained with a lower threshold of 50 keV. The comparison of three crystals showed that 1.5 mm thick crystal had higher overall sensitivity compared to 1.0 mm crystal ($p < 0.05$) and 0.5 mm crystal ($p < 0.05$). However, the 0.5 mm thick crystal was most insensitive to gamma radiation compared to the other two crystals ($p < 0.05$), and it had a beta sensitivity comparable to them. Thus, in terms of beta to gamma detection ratio, a crystal thickness of the 0.5 mm was found to be optimum ($p < 0.05$).

Table 7. Comparison of three thicknesses of $\text{CaF}_2(\text{Eu})$ crystal in terms of beta to gamma detection ratio.

Crystal Thickness (mm)	Overall counts (CPS/kBq)*	Photon counts (CPS/kBq)	Beta counts (CPS/kBq)	Ratio (Beta/Photon)
0.5	19 ± 2	2.1 ± 0.1	17 ± 2	8.1 ± 0.7
1.0	22 ± 3	3.8 ± 0.6	19 ± 2	4.9 ± 0.3
1.5	24 ± 3	5.3 ± 0.8	19 ± 2	3.6 ± 0.4

*CPS/kBq - counts per second per kilo Becquerel

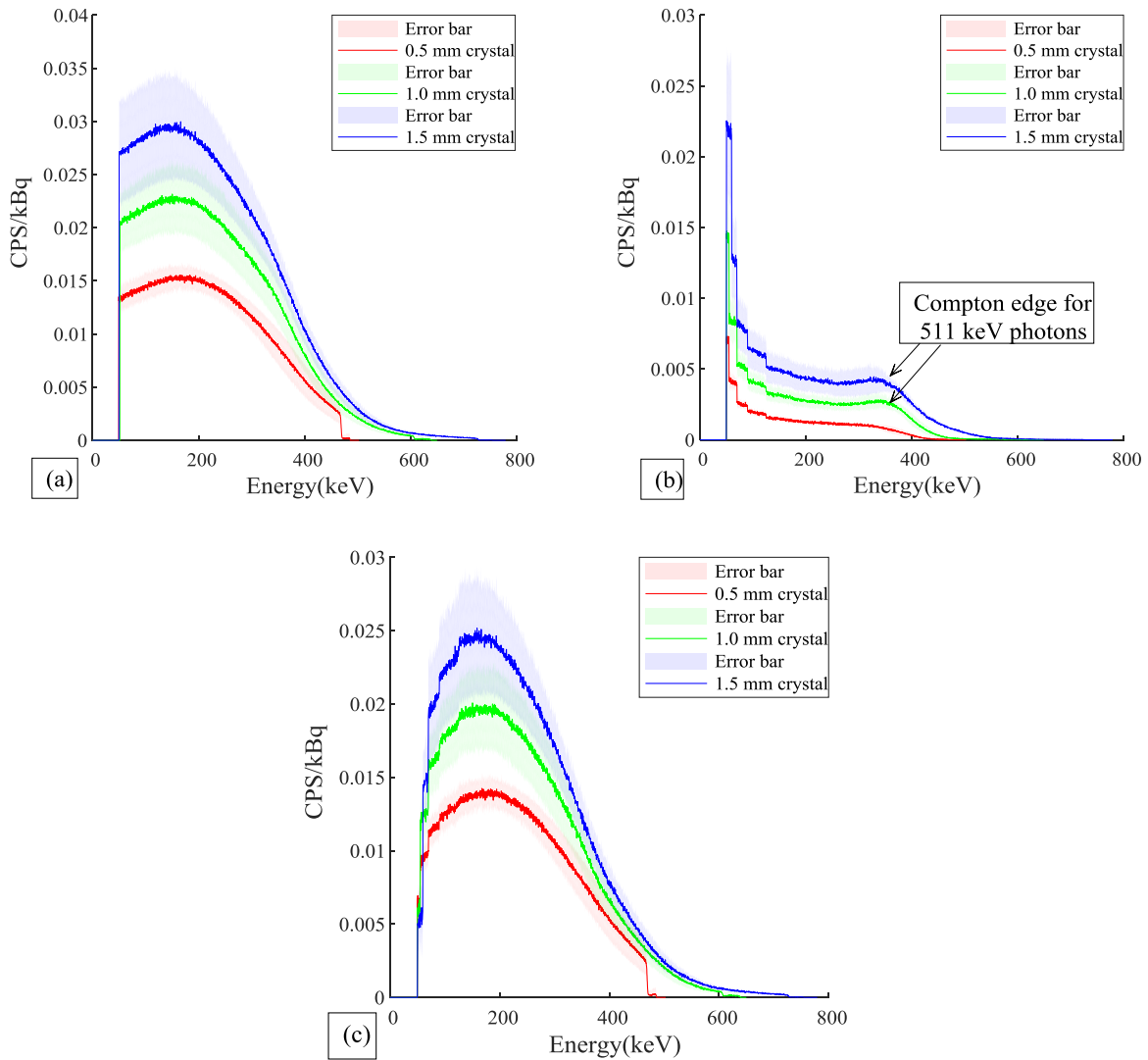


Figure 6. (a) Overall spectra obtained with three $\text{CaF}_2(\text{Eu})$ crystals by exposing detectors to the ^{18}F -FDG source. (b) Photon spectra obtained with three $\text{CaF}_2(\text{Eu})$ crystals of different thickness by stopping beta particles with a 0.56 mm thick copper sheet along with photon attenuation correction in the copper sheet. (c) Beta spectrums for three crystals obtained by the subtraction of the corresponding photon spectrum from the overall spectrum for all three crystals. Data presented in plots is the average of six measurements and the error bars were generated by accounting for the standard deviation in CPS/kBq at all energies.

2.4.2 Detector sensitivity map

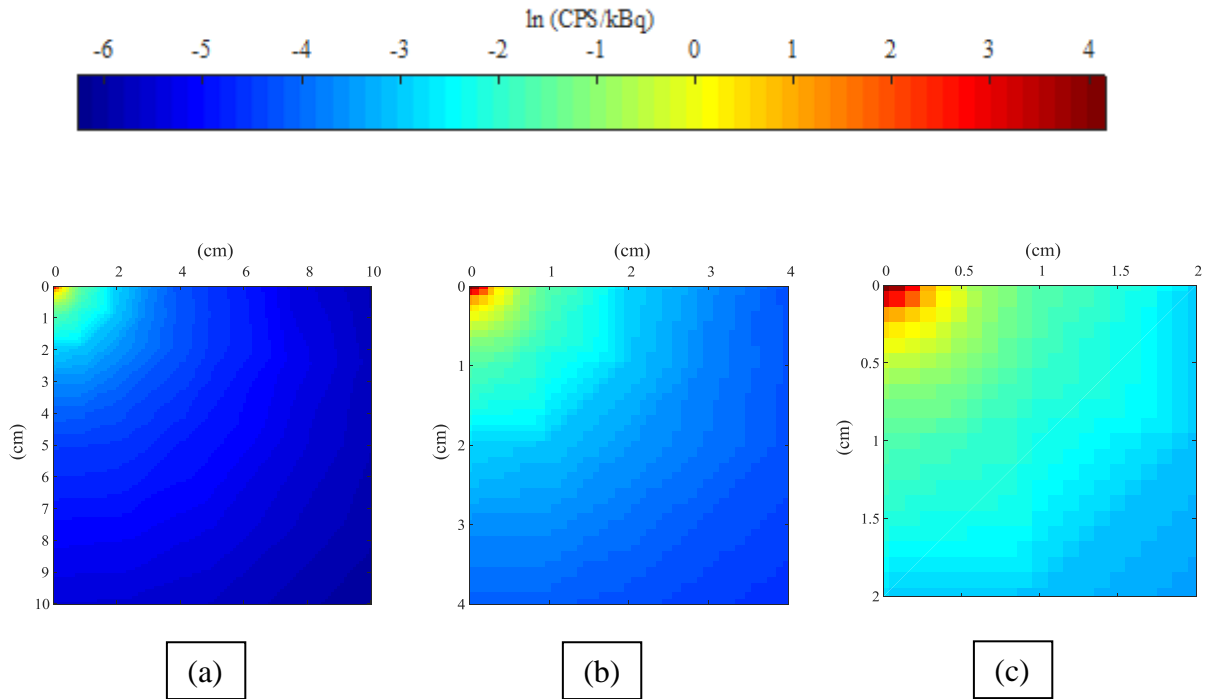


Figure 7. Graphical representation of the 2D sensitivity map of the beta sensitive detector for the ^{18}F -FDG source. Figure (a) represents detector sensitivity map in a region of $10 \times 10 \text{ cm}^2$, which is average of five measurements, Figure (b) represents average detector sensitivity map in a region of $4 \times 4 \text{ cm}^2$, and Figure (c) represents average detector sensitivity map in a region of $2 \times 2 \text{ cm}^2$. Horizontal and vertical axis represent the source translation parallel to the detector and in depth in water tank in centimetres, respectively.

Figure 7(a) represents the 2D detector sensitivity map. The upper left corner of the map corresponds to the detector sensitivity of $62 \pm 3 \text{ CPS/kBq}$, where the source was placed at the center of the detector at a distance of 0 cm from the detector. The farthest point at the lower right corner represents sensitivity at a depth of 10 cm and an axial displacement of 10 cm. Figure 8 shows that the sensitivity drops rapidly with an increase in the source to detector distance, which is desirable to reduce the detection of background radiation.

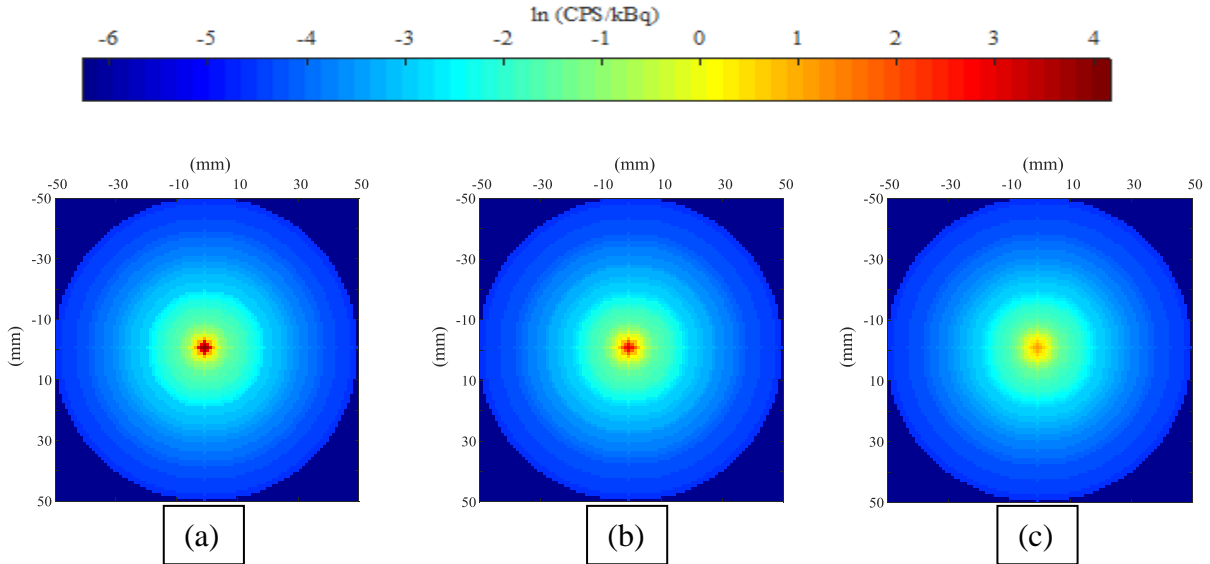


Figure 8. The rapid fall of detector sensitivity with an increase in distance of the source from the detector. Figure (a), (b), and (c), represent the first three slices of the 3D detection sensitivity map at the depth of 0 mm, 1 mm, and 2 mm, respectively. Axes represent the position of pixels in the slice in centimetres with respect to the origin at the centre of the slice.

2.4.3 Minimum detectable tumour surface area (MDTSA)

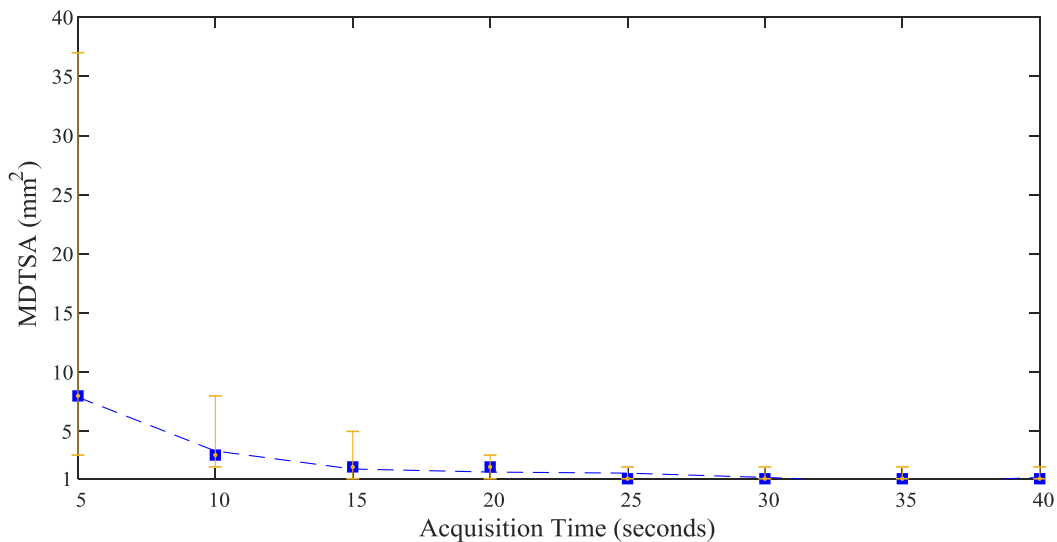


Figure 9. The effect of increasing acquisition time on the MDTSA for ^{18}F -FDG with the T:B ratio fixed at 7. The error bars in the plot were generated by considering the variation of normal breast tissue activity in patients. The dotted curve is obtained through the least square curve fitting to data points.

Figure 9 represents the effect of increasing acquisition time on the MDTSA for the radiopharmaceutical ^{18}F -FDG with the T:B ratio fixed at 7 and normal breast tissue activity fixed at 1.69 kBq/ml. It is observed that MDTSA decreases (inversely proportional to the square root of acquisition time) with an increase in acquisition time. For patients with similar experimental conditions, it is expected that with an acquisition time of 25 seconds, 10 mm long cancerous tendril with a 1 mm^2 cross-sectional area at the cut edge of excised tissue can be detected.

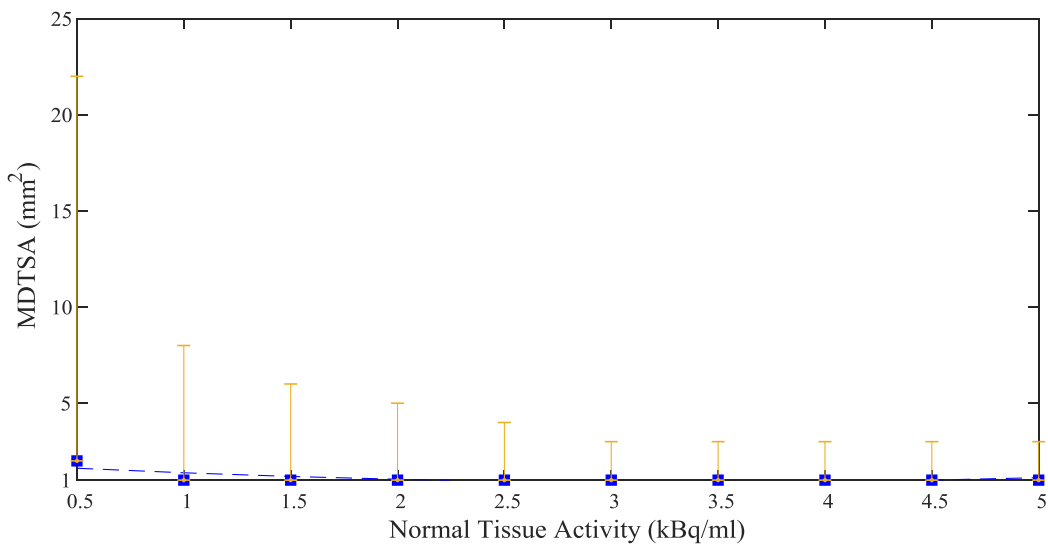


Figure 10. The effect of increasing breast normal tissue activity on the MDTSA for ^{18}F -FDG. Acquisition time was fixed at 30 seconds. The error bars in the plot were generated by considering the variation of the T:B ratio in the patients. The dotted curve is obtained by the least square curve fit.

The plot in Figure 10 illustrates the variation of the MDTSA with the increase in normal breast tissue radioactivity concentration at a fixed acquisition time of 30 seconds and the T:B ratio fixed at 7. The plot shows that with normal breast tissue activity of 1.0 kBq/ml, detection of 10 mm long cancerous tendril with a cross-sectional area of 1 mm^2 at the cut edge of excised tissue is feasible, in patients who satisfy the experimental conditions.

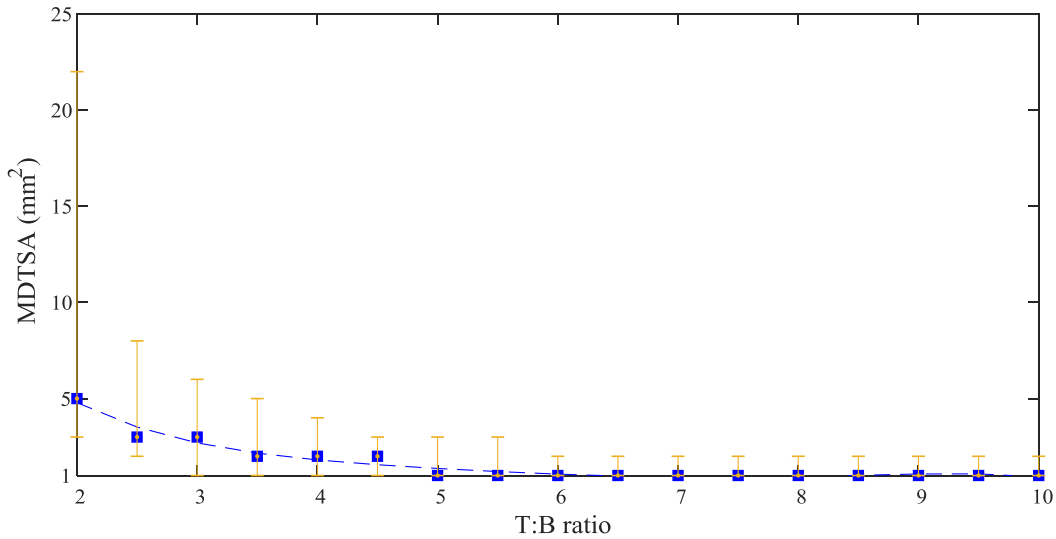


Figure 11. The effect of increasing the T:B ratio on the MDTSA for ^{18}F -FDG. Acquisition time was fixed at 30 seconds. The error bars in the plot were generated by considering the variation of normal breast tissue activity in patients. The dotted curve is obtained by the least square curve fitting to data points.

Figure 11 represents the variation of MDTSA with the variation of T:B ratio. The plot shows that with an acquisition time specified at 30 seconds, normal tissue activity fixed at 1.69 kBq/ml, and the T:B ratio of 5, detection of 10 mm long cancerous tendril with a cross-sectional area 1 mm² at the cut edge of excised tissue is feasible. For the patients with similar experimental conditions, it is expected that with the T:B ratio higher than 5, less than 1 mm² cancerous deposits at the surface of surgically removed specimen can be detected.

2.5 Discussion

Presently, BCS suffer from a lack of intra-operative guidance. In this work, a prototype single pixel beta sensitive detector was successfully developed and evaluated for its potential as an intra-operative guidance tool. The final incarnation of the device will consist of an array of the single pixel prototype developed in this study. The purpose of this device will be to detect cancerous deposits at the cut edge of the surgically excised cancerous breast tissue.

The scintillation crystal thickness was optimized to make the detector less sensitive to gamma ray photons compared to beta particles. The experimental results of the crystal thickness optimization study are similar to the results obtained by Tornai et al. [92]. According to a

simulation, Tornai determined that the $\text{CaF}_2(\text{Eu})$ scintillation crystal thickness of 0.6 mm is optimum for beta particle detection and imaging. However, due to the unavailability of a 0.6 mm crystal, a 0.5 mm crystal was used in the present study. The optimized crystal has a good beta to gamma detection ratio, which indicates the detector is suitable to detect beta particles without requiring additional gamma rejection strategies.

The single pixel detector has an expected detection sensitivity of 7 CPS/kBq with an effective area of 1 mm^2 , which is significantly higher than the sensitivity of existing beta particle detectors. The existing beta sensitive detectors and probes have detection sensitivities of 0.5 CPS/kBq [86], 0.9 CPS/kBq [80], 0.01 CPS/kBq [82] with a 1 mm^2 effective area. The detector developed by Spadola et al., based on p-Terphenyl scintillator, has shown on phantom evaluations to be able to reliably detect a 3 mm diameter tumour [86]. Additionally, a Monte Carlo simulation based study estimates a 5 mm diameter and 3 mm thick p-Terphenyl scintillator detector can detect 0.1 ml of cancer tissue for imaging times greater than 25 seconds [115].

The sensitivity of the newly developed beta detector is well suited to the task of detecting superficial involvement of an excised tissue sample, as the detector sensitivity decreases sharply with an increase in distance between the detector and the ^{18}F -FDG source. It reduces from 62 ± 3 CPS/kBq to 1.6 ± 0.3 CPS/kBq as the distance increases from 0 mm to 3 mm. The drop in detection efficiency with the increase in separation is the result of the short range of beta particles in water.

The *in silico* study presented above suggests that the novel beta detector could be capable of detecting 10 mm long cancerous tendril with a 1 mm^2 cross-sectional area at the cut edge of excised tissue in a clinically reasonable time. The *in silico* tumour model used in this study was designed to represent the worst case scenario for detecting tumour deposits, where the involvement at the surface of the excised tissue sample was made to correspond with the diameter of a single milk duct. The normal breast tissue activity and T:B ratios used for the modelling exercise were selected to be a representative of the range reported in the literature using SUV. A limitation with using these estimates is that SUV is based on a bulk average as measured using positron emission tomography, which cannot resolve the uptake differences measured at the scale of the beta detector.

The current detector is a single pixel detector, and additional validation is required to determine whether the performance reported in this study remains when the single pixel prototype is arrayed to make a multi-pixel detector and imager. Furthermore, the focus of future studies will be to characterize the response of the device using animal models of breast cancer.

2.6 Conclusion

In this work, a prototype single pixel beta detector was developed, consisting of a $\text{CaF}_2(\text{Eu})$ scintillation crystal optically coupled to a SiPM. The thickness of the scintillation crystal was altered to optimize the beta sensitivity and photon insensitivity of the detector. Additionally, in an *in silico* study, the detector was evaluated for its potential use as an intra-operative guidance tool in BCS. The novel beta sensitive detector has the potential to detect 10 mm long cancerous tendril with a less than 1 mm^2 cross-sectional area at the cut edge of surgically removed cancerous tissue, in a clinically reasonable time. This *in silico* study uses a computer model of the detector response, which was obtained in water. Water has electron density and effective atomic number comparable to that of breast tissue. Thus, significance differences between the result from this present study and *in vivo* evaluation are not expected.

Based on the result of the present study a $10 \times 10 \text{ cm}^2$ scanner will be developed and validated using an animal model of breast cancer. Successful application of the detector in BCS will be dependent on the type of tumour, the radiopharmaceutical, uptake in the tumour and clearance of activity in the healthy tissue.

2.7 Acknowledgements

This work was funded by a research grant from Cancer Imaging Network of Ontario.

Chapter 3 Conclusion

3.1 Thesis overview

The focus of the thesis was to develop a single pixel beta sensitive detector and to evaluate its performance to detect $< 1 \text{ mm}^2$ deposits of cancer cells at the cut edge of the surgically removed cancerous breast tissue. To address the incomplete surgery, 6-55% of patients with a breast-conserving surgery (BCS) undergo a re-excision [43-45]. The main reason for the high rate of re-excision is the poor intra-operative guidance available to the surgical oncologist. Thus, an intra-operative image guidance technique is required.

The existing procedures such as palpation, wire guided localization, intra-operative ultrasound guided surgeries, and radioactive seed localization, do not provide any information of the tumour edges. Additionally, they are associated with high rates of a positive and close tumour margin. Radio-immuno guided surgery could have the potential to solve this problem, but it suffers from high background radiation originating from nonspecific uptake of the radiopharmaceutical in distal organs [101]. A beta particle guided surgery takes advantage of the short range of beta particles in tissue. This minimizes the possibility of detection of beta particles from distal organs. Thus, a beta particle based intra-operative surgical margin evaluation tool could potentially improve surgical outcomes of BCS.

Chapter 2 describes the novel beta particle detector construction, and results from an *in silico* modelling study of the detector response to identify cancerous deposits at the cut edge of the surgically removed cancerous breast tissue. The purpose of this evaluation was to determine whether the beta particle detector could detect, with a sensitivity of 95%, involvement of the tumour margin.

Firstly, during the detector development phase, the thickness of the scintillation element of the detector was optimized to improve background noise rejection. The $\text{CaF}_2(\text{Eu})$ crystal of a thickness of 0.5 mm provided a superior beta to gamma detection ratio. This crystal was used in the final detector assembly and it was directly coupled to a silicon photomultiplier (SiPM). Although as a small size ($3 \times 3 \text{ mm}^2$) detector, it has a detection efficiency of $62 \pm 3 \text{ CPS/kBq}$. Furthermore, a three-dimensional sensitivity map of the detector response was acquired with a ^{18}F -FDG point source. Using a computerized model of this map and a simulated clinically realistic excised breast cancerous tissue, an *in silico* study showed that with a normal breast tissue activity as small as 1.69 kBq/ml and the T:B ratio of 5, 10 mm long cancerous tendril with a cross-sectional area $< 1 \text{ mm}^2$, can be detected at the cut edge of the surgically excised

specimen in a clinically acceptable time of 30 seconds. Thus, beta guided surgeries using a $\text{CaF}_2(\text{Eu})$ scintillation detector may become a useful tool for intra-operative guidance during BCS.

3.2 Discussion and future work

A $\text{CaF}_2(\text{Eu})$ scintillator-based detector was evaluated as a part of this thesis and it was found to be suitable for intra-operative tumour margin evaluation. However, there may be potential to further improve the performance of this prototype device by evaluating different scintillating crystals. In order to improve performance, a replacement crystal must have the following properties: a low atomic number, high scintillation light yield, and transparency to the scintillation light.

A doped p-Terphenyl organic scintillating crystal has a high light yield of the order of 33000 photons/MeV [116], which makes it a highly attractive alternate crystal to $\text{CaF}_2(\text{Eu})$ which has a light yield of 24000 photons/MeV. However, the main limitation of p-Terphenyl is its high self-attenuation of the scintilla that it produces. It has a short attenuation length of 3.89 mm [116] compared to the attenuation length of the $\text{CaF}_2(\text{Eu})$ of 2 - 5 cm. Previously published results from Monte Carlo simulations show that the p-Terphenyl scintillator have a poor detection sensitivity below 400 keV beta particle energies [87,115] whereas the most of the beta particles emitted by ^{18}F have an energy less than 400 keV. Nonetheless, researchers have attempted to exploit the p-Terphenyl scintillator [86,88]. Spadola et al. reported the detection of a 3 mm diameter brain tumour in phantom studies with an imaging time of approximately 10 seconds using a 0.1 mm thick p-Terphenyl scintillator [86]. Another probe developed by Camillocci et al. consisting of a 3 mm thick p-Terphenyl scintillator [88], had a poor detection sensitivity for beta particles emitted by ^{18}F compared to a thin scintillator, which can be due to self attenuation of the p-Terphenyl. Even though a $\text{CaF}_2(\text{Eu})$ scintillator-based beta detector has better performance compared to the p-Terphenyl probes that have been reported, it may be prudent to optimize the crystal thickness of p-Terphenyl for its application in intra-operative margin evaluation.

The future study consists of optimization of p-Terphenyl scintillator thickness for superior beta to gamma detection ratio and evaluation of p-Terphenyl scintillator with optimized thickness to determine minimum detectable tumour surface area. The result of this future study

will be compared to the result of the present study. The superior scintillator with optimized thickness will be used to develop a four pixel detector to determine the impact of detector scaling on its performance. Further a large area scanner will be constructed to cover an area of $10 \times 10 \text{ cm}^2$ consisting of a monolithic layer of the optimized scintillator optically coupled to a two-dimensional array of silicon photomultipliers. The Anger logic will be used to determine the position of interaction of beta particles in the scintillator. This novel scanner will be used to examine entire margins of the surgically excised cancerous breast tissue. Before proceeding to clinical trials, the scanner will be characterized using animal models of breast cancer.

The presence of tumour in an animal will be confirmed with radiological diagnosis prior to the experimentation. The animal will be injected with 2-Deoxy-2-[18F] Fluoroglucose and the surgically excised tumour with different sutures on different faces will be obtained. Immediately, all faces of the excised tumour will be imaged with the $10 \times 10 \text{ cm}^2$ imager and the sutures will represent the orientation of the excised tissue. Afterwards, the sample will be sent for pathological evaluation and results of the pathological evaluation will be correlated to findings of the imager. Based on the result of the present study, it is expected that the imager will be capable of imaging microscopic cancer present at cut edges of the excised cancerous specimen.

Appendix

A1 Tumour Model

Surgically excised tissue was modelled in MATLAB (MATLAB 9.2, MathWorks, Inc., Natick, MA, US). The modelling of an excised specimen consisted of an ellipsoidal cancerous tissue with semi axes (1.5 cm, 1.5 cm, and 1.00 cm) which was surrounded by a shell of 1.0 cm thick healthy tissue. This model is representative of a typical early stage breast cancer tumour that has been excised. Each voxel in the simulated excised tissue was labelled as healthy tissue or cancerous tissue and was populated with the appropriate ^{18}F -FGD activity.

A2 Tumour growth

Breast cancerous tissue do not have clearly visible round border. Pathological evaluation of the excised tissue reveals that breast cancer possess spiculated structure at the borders [42]. This may be because of the presence of ductal carcinoma in situ (DCIS) component with invasive ductal carcinoma (IDC). Mostly, IDC has an associated DCIS [117]. DCIS is confined within milk ducts [4] and the diameter of milk ducts in a breast varies from 1.2 - 2.5 mm [104]. The focus of this study was the detection of cancer within the milk duct, which are difficult for a surgical oncologist to detect during surgery. Thus, in the computer model of the excised tissue, the tumour growth was simulated as a tendril of $1 \times 1 \times 10 \text{ mm}^3$ at each iteration. This geometry of tumour growth was simulated because a tendril is hard to detect compared to 10 mm^3 tissue exactly at the cut edge. For a 10 mm^3 cancerous tissue exactly at the cut edge, maximum beta particles can reach the detector which makes the detection favourable. However, in case of a $1 \times 1 \times 10 \text{ mm}^3$ tendril a limited number of beta particles will be able to reach the detector because of their limited range in tissue. This makes the detection of tumour cells at edges of excised tissue challenging.

Bibliography

- [1] Canadian Cancer Society, Canadian Cancer Society's Advisory Committee on Cancer Statistics : Canadian Cancer Statistics 2017, Toronto, 2017.
- [2] J. Ferlay, I. Soerjomataram, R. Dikshit, S. Eser, C. Mathers, M. Rebelo, D.M. Parkin, D. Forman, F. Bray, Cancer incidence and mortality worldwide: Sources, methods and major patterns in GLOBOCAN 2012, *Int. J. Cancer*. 136 (2015) E359–E386.
doi:10.1002/ijc.29210.
- [3] M. Shields, K. Wilkins, An update on mammography use in Canada, *Heal. Reports*. 20 (2009) 7–19. doi:82-003-XPE.
- [4] Canadian Cancer Society, Types of Breast Cancer, (2017).
<http://www.cbcf.org/central/aboutbreastcancermain/diagnosis/pages/breastcancertypes.aspx> (accessed May 5, 2018).
- [5] M.P. Barbara S. Hulka, Reprint of breast cancer: hormones and other risk factors, *Maturitas*. 61 (2008) 203–214. doi:10.1016/j.maturitas.2008.11.016.
- [6] K. McPherson, C.M. C M Steel, J.M. Dixon, Breast cancer-epidemiology, risk factors, and genetics, *Br. Med. J.* 309 (1994) 1003–1006.
- [7] M. Khalis, B. Charbotel, V. Chajès, S. Rinaldi, A. Moskal, C. Biessy, L. Dossus, I. Huybrechts, E. Fort, N. Mellas, S. Elfakir, H. Charaka, C. Nejjari, I. Romieu, K. El Rhazi, Menstrual and reproductive factors and risk of breast cancer: A case-control study in the Fez region, Morocco, *PLoS One*. 13 (2018) e0191333.
doi:10.1371/journal.pone.0191333.
- [8] M. Lambertini, L. Santoro, L. Del Mastro, B. Nguyen, L. Livraghi, D. Ugolini, F.A. Peccatori, H.A. Azim, Reproductive behaviors and risk of developing breast cancer according to tumor subtype: A systematic review and meta-analysis of epidemiological studies, *Cancer Treat. Rev.* 49 (2016) 65–76. doi:10.1016/j.ctrv.2016.07.006.
- [9] M.P. Madigan, R.G. Ziegler, J. Benichou, C. Byrne, R.N. Hoover, Proportion of breast cancer cases in the United States explained by well-established risk factors, *J. Natl. Cancer Inst.* 87 (1995) 1681–1685. doi:10.1093/jnci/87.22.1681.
- [10] M.J. Adams, A. Dozier, R.E. Shore, S.E. Lipshultz, R.G. Schwartz, L.S. Constine, T.A.

- Pearson, M. Stovall, P. Winters, S.G. Fisher, Breast cancer risk 55+ years after irradiation for an enlarged thymus and its implications for early childhood medical irradiation today, *Cancer Epidemiol. Biomarkers Prev.* 19 (2010) 48–58. doi:10.1158/1055-9965.EPI-09-0520.
- [11] W.D. Thompson, Genetic epidemiology of breast cancer, *Cancer.* 74 (1994) 279–287. doi:10.1002/cncr.2820741312.
- [12] K.M.J. De Bruijn, L.R. Arends, B.E. Hansen, S. Leeflang, R. Ruiter, C.H.J. Van Eijck, Systematic review and meta-analysis of the association between diabetes mellitus and incidence and mortality in breast and colorectal cancer, *Br. J. Surg.* 100 (2013) 1421–1429. doi:10.1002/bjs.9229.
- [13] H.K. Seitz, C. Pelucchi, V. Bagnardi, C. La Vecchia, Epidemiology and pathophysiology of alcohol and breast cancer: Update 2012, *Alcohol Alcohol.* 47 (2012) 204–212. doi:10.1093/alcalc/ags011.
- [14] J. Luo, K.L. Margolis, J. Wactawski-Wende, K. Horn, C. Messina, M.L. Stefanick, H.A. Tindle, E. Tong, T.E. Rohan, Association of active and passive smoking with risk of breast cancer among postmenopausal women: a prospective cohort study, *BMJ.* 342 (2011) 536. doi:10.1136/bmj.d1016.
- [15] Canadian Cancer Society, Survival statistics for breast cancer, (2018). <http://www.cancer.ca/en/cancer-information/cancer-type/breast/prognosis-and-survival/survival-statistics/?region=on> (accessed May 25, 2018).
- [16] T. Zuo, H. Zeng, H. Li, S. Liu, L. Yang, C. Xia, R. Zheng, F. Ma, L. Liu, N. Wang, L. Xuan, W. Chen, The influence of stage at diagnosis and molecular subtype on breast cancer patient survival: a hospital-based multi-center study, *Chin. J. Cancer.* 36 (2017) 84. doi:10.1186/s40880-017-0250-3.
- [17] I.K. Larsen, T.Å. Myklebust, T.B. Johannesen, B. Møller, S. Hofvind, Stage-specific incidence and survival of breast cancer in Norway: The implications of changes in coding and classification practice, *Breast.* 38 (2018) 107–113. doi:10.1016/j.breast.2017.12.001.
- [18] S.A. Narod, J. Iqbal, A.B. Miller, Why have breast cancer mortality rates declined?, *J. Cancer Policy.* 5 (2015) 8–17. doi:10.1016/j.jcpo.2015.03.002.
- [19] E. Vilapriyo, T. Puig, M. Rue, Contribution of early detection and adjuvant treatments to breast cancer mortality reduction in Catalonia, Spain, *PLoS One.* 7 (2012) e30157.

- doi:10.1371/journal.pone.0030157.
- [20] S. Hofvind, B.M. Geller, J. Skelly, P.M. Vacek, Sensitivity and specificity of mammographic screening as practised in Vermont and Norway, *Br. J. Radiol.* 85 (2012) e-1226-e1232. doi:10.1259/bjr/15168178.
- [21] M.T. Mandelson, N. Oestreicher, P.L. Porter, D. White, C.A. Finder, S.H. Taplin, E. White, Breast density as a predictor of mammographic detection: Comparison of interval and screen detected cancers, *J. Natl. Cancer Inst.* 92 (2000) 1081–1087. doi:10.1093/jnci/92.13.1081.
- [22] T.B. Bevers, Ultrasound for the screening of breast cancer, *Curr. Sci. Inc.* 10 (2008) 527–528. doi:10.1007/s11912-008-0079-7.
- [23] W. Buchberger, S. Geiger-Gritsch, R. Knapp, K. Gautsch, W. Oberaigner, Combined screening with mammography and ultrasound in a population-based screening program, *Eur. J. Radiol.* 101 (2018) 24–29. doi:10.1016/j.ejrad.2018.01.022.
- [24] C. Lehman, C. Isaacs, M. Schnall, E. Pisano, S. Ascher, E. Al., Cancer yield of mammography, MR, and US in high-risk women: prospective multi-institution breast cancer screening study, *Radiology.* 244 (2007) 381–388. doi:10.1148/radiol.2442060461.
- [25] C. Kuhl, S. Weigel, S. Schrading, B. Arand, H. Bieling, R. König, B. Tombach, C. Leutner, A. Rieber-Brambs, D. Nordhoff, W. Heindel, M. Reiser, H.H. Schild, Prospective multicenter cohort study to refine management recommendations for women at elevated familial risk of breast cancer: The EVA trial, *J. Clin. Oncol.* 28 (2010) 1450–1457. doi:10.1200/JCO.2009.23.0839.
- [26] A.K. Narayan, K. Visvanathan, S.C. Harvey, Comparative effectiveness of breast MRI and mammography in screening young women with elevated risk of developing breast cancer: a retrospective cohort study, *Breast Cancer Res. Treat.* 158 (2016) 583–589. doi:10.1007/s10549-016-3912-y.
- [27] W. DeMartini, C. Lehman, S. Partridge, Breast MRI for cancer detection and characterization. A review of evidence-based clinical applications, *Acad. Radiol.* 15 (2008) 408–416. doi:10.1016/j.acra.2007.11.006.
- [28] D.L. Monticciolo, M.S. Newell, L. Moy, B. Niell, B. Monsees, E.A. Sickles, Breast cancer screening in women at higher-than-average risk: recommendations from the ACR, *J. Am. Coll. Radiol.* 15 (2018) 408–414. doi:10.1016/j.jacr.2017.11.034.

- [29] NCCN, Breast cancer screening and diagnosis, *Compr. Cancer*. (2009) 1–56. doi:10.1007/978-1-4939-1267-4.
- [30] W.A. Berg, L. Gutierrez, M.S. Nessler, W.B. Carter, M. Bhargavan, R.S. Lewis, O.B. Ioffe, Diagnostic accuracy of mammography, clinical examination, US, and MR imaging in preoperative assessment of breast cancer, *Radiology*. 233 (2004) 830–849. doi:10.1148/radiol.2333031484.
- [31] C.E. Redmond, G.M. Healy, C.F. Murphy, A. O’Doherty, A. Foster, The use of ultrasonography and digital mammography in women under 40 years with symptomatic breast cancer: a 7-year Irish experience, *Ir. J. Med. Sci.* 186 (2017) 63–67. doi:10.1007/s11845-016-1472-0.
- [32] T. Anusinha, W. Tangcharoensathien, S. Rattanamongkolgul, T. Srianjata, S. Mayurasakorn, Effect of age on performance parameters of screening and diagnostic mammography examinations, *Siriraj Med. J.* 68 (2016) 6–16.
- [33] P.B. Gordon, S.L. Goldenberg, Malignant breast masses detected only by ultrasound. A retrospective review, *Cancer*. 76 (1995) 626–630. doi:10.1002/1097-0142(19950815)76:4<626::AID-CNCR2820760413>3.0.CO;2-Z.
- [34] X. Ying, Y. Lin, X. Xia, B. Hu, Z. Zhu, P. He, A comparison of mammography and ultrasound in women with breast disease: a receiver operating characteristic analysis, *Breast J.* 18 (2012) 130–138. doi:10.1111/j.1524-4741.2011.01219.x.
- [35] N. Bruck, I. Koskivuo, P. Bostrom, J. Saunavaara, Preoperative magnetic resonance imaging in patients with stage I invasive ductal breast cancer: a prospective randomized study, *Scand. J. Surg.* 107 (2018) 14–22. doi:10.1177/1457496917701669.
- [36] J.H. Menell, E.A. Morris, D.D. Dershaw, A.F. Abramson, E. Brogi, L. Liberman, Determination of the presence and extent of pure ductal carcinoma in situ by mammography and magnetic resonance imaging, *Breast J.* 11 (2005) 382–390. doi:10.1111/j.1075-122X.2005.00121.x.
- [37] E.S. Hwang, K. Kinkel, L.J. Esserman, Y. Lu, N. Weidner, N.M. Hylton, Magnetic resonance imaging in patients diagnosed with ductal carcinoma-in-situ: value in the diagnosis of residual disease, occult invasion, and multicentricity., *Ann. Surg. Oncol.* 10 (2003) 381–8. doi:10.1245/ASO.2003.03.085.
- [38] American Cancer Society, *Breast Cancer Facts & Figures 2017-2018*, Atlanta, 2017.

- [39] E.B.C.T.C.G. Early Breast Cancer Trialists' Collaborative Group (EBCTCG), S. Darby, P. McGale, C. Correa, C. Taylor, R. Arriagada, M. Clarke, D. Cutter, C. Davies, M. Ewertz, J. Godwin, R. Gray, L. Pierce, T. Whelan, Y. Wang, R. Peto, Effect of radiotherapy after breast-conserving surgery on 10-year recurrence and 15-year breast cancer death: meta-analysis of individual patient data for 10,801 women in 17 randomised trials, *Lancet* (London, England). 378 (2011) 1707–16. doi:10.1016/S0140-6736(11)61629-2.
- [40] S.L. Blair, K. Thompson, J. Rococco, V. Malcarne, P.D. Beitsch, D.W. Ollila, Attaining negative margins in breast-conservation operations: Is there a consensus among breast surgeons?, *J. Am. Coll. Surg.* 209 (2009) 608–613. doi:10.1016/j.jamcollsurg.2009.07.026.
- [41] U.S. Food and Drug Administration, Guidance for industry: pathological complete response in neoadjuvant treatment of high-risk early-stage breast cancer: Use as an endpoint to support accelerated approval. October 2014, Silver Spring, 2014. <http://www.fda.gov/Drugs/GuidanceComplianceRegulatoryInformation/Guidances/default.htm>.
- [42] D. Carter, Margins of “Lumpectomy” for breast cancer, *Hum. Pathol.* 17 (1986) 330–332. doi:10.1016/S0046-8177(86)80455-5.
- [43] A.K. Talsma, A.M.J. Reedijk, R.A.M. Damhuis, P.J. Westenend, W.J. Vles, Re-resection rates after breast-conserving surgery as a performance indicator: Introduction of a case-mix model to allow comparison between Dutch hospitals, *Eur. J. Surg. Oncol.* 37 (2011) 357–363. doi:10.1016/j.ejso.2011.01.008.
- [44] L.E. McCahill, R.M. Single, E.J. Aiello Bowles, H.S. Feigelson, T.A. James, T. Barney, J.M. Engel, A.A. Onitilo, Variability in reexcision following breast conservation surgery, *JAMA.* 307 (2012) 467. doi:10.1001/jama.2012.43.
- [45] J.M. Escribà, L. Esteban, J. Gálvez, M.J. Pla, A. Melià, M. Gil-Gil, R. Clèries, L. Pareja, X. Sanz, M. Bustins, J.M. Borràs, J. Ribes, Reoperations after primary breast conserving surgery in women with invasive breast cancer in Catalonia, Spain: a retrospective study, *Clin. Transl. Oncol.* 19 (2017) 448–456. doi:10.1007/s12094-016-1546-5.
- [46] N.M. Krekel, B.M. Zonderhuis, H.W. Schreurs, A.M. Lopes Cardozo, H. Rijna, H. van der Veen, S. Muller, P. Poortman, L. de Widt, W.K. de Roos, A.M. Bosch, A.H. Taets

- van Amerongen, E. Bergers, M.H. van der Linden, E.S. de Lange de Klerk, H.A. Winters, S. Meijer, P.M. van den Tol, Ultrasound-guided breast-sparing surgery to improve cosmetic outcomes and quality of life. A prospective multicentre randomised controlled clinical trial comparing ultrasound-guided surgery to traditional palpation-guided surgery (COBALT trial), *BMC Surg.* 11 (2011) 8. doi:10.1186/1471-2482-11-8.
- [47] N. Krekel, B. Zonderhuis, S. Muller, H. Bril, H.J. Van Slooten, E. De Lange De Klerk, P. Van Den Tol, S. Meijer, Excessive resections in breast-conserving surgery: A retrospective multicentre study, *Breast J.* 17 (2011) 602–609. doi:10.1111/j.1524-4741.2011.01198.x.
- [48] R.G. Pleijhuis, M. Graafland, J. de Vries, J. Bart, J.S. de Jong, G.M. van Dam, Obtaining adequate surgical margins in breast-conserving therapy for patients with early-stage breast cancer: current modalities and future directions., *Ann. Surg. Oncol.* 16 (2009) 2717–2730. doi:10.1245/s10434-009-0609-z.
- [49] S. van Esser, M.G. Hobbelink, P.H. Peeters, E. Buskens, I.M. van der Ploeg, W.P. Mali, I.H.M.B. Rinkes, R. van Hillegersberg, The efficacy of “Radio guided Occult Lesion Localization” (ROLL) versus “Wire-guided Localization” (WGL) in breast conserving surgery for non-palpable breast cancer: A randomized clinical trial – ROLL study, *BMC Surg.* 8 (2008) 9. doi:10.1186/1471-2482-8-9.
- [50] S.H. Javid, L.J. Kirstein, E. Rafferty, S. Lipsitz, R. Moore, J.E. Rusby, C.D. Murphy, K.S. Hughes, M.C. Specht, A.G. Taghian, B.L. Smith, Outcome of multiple-wire localization for larger breast cancers: do multiple wires translate into additional imaging, biopsies, and recurrences?, *Am. J. Surg.* 198 (2009) 368–372. doi:10.1016/j.amjsurg.2009.01.021.
- [51] H.C. Burkholder, L.E. Witherspoon, R.P. Burns, J.S. Horn, M.D. Biderman, Breast surgery techniques: Preoperative bracketing wire localization by surgeons, *Am. Surg.* 73 (2007) 574–578.
- [52] H. Eggemann, S.D. Costa, A. Ignatov, Ultrasound-guided versus wire-guided breast-conserving surgery for nonpalpable breast cancer, *Clin. Breast Cancer.* 16 (2016) e1–e6. doi:10.1016/j.clbc.2015.09.001.
- [53] L. Langhans, M.B. Jensen, M.L.M. Talman, I. Vejborg, N. Kroman, T.F. Tvedskov, Reoperation rates in ductal carcinoma in situ vs invasive breast cancer after wire-guided

- breast-conserving surgery, *JAMA Surg.* 152 (2017) 378–384.
doi:10.1001/jamasurg.2016.4751.
- [54] L. Langhans, T.F. Tvedskov, T.L. Klausen, M.B. Jensen, M.L. Talman, I. Vejborg, C. Benian, A. Roslind, J. Hermansen, P.S. Oturai, N. Bentzon, N. Kroman, Radioactive seed localization or wire-guided localization of nonpalpable invasive and in situ breast cancer: A randomized, multicenter, open-label trial, *Ann. Surg.* 266 (2017) 29–35.
doi:10.1097/SLA.0000000000002101.
- [55] D. Ocal Koray, Dag Ahmet, Turkmenoglu Ozgur, Gunay Emel Ceylan, Yucel Erdem, and M. Nass, Radioguided occult lesion localization versus wire-guided localization for non-palpable breast lesions: randomized controlled trial, *Clinics.* 66 (2011) 1003–1007.
doi:10.1590/S1807-59322011000600014.
- [56] A. Haid, M. Knauer, S. Dunzinger, Z. Jasarevic, R. Köberle-Wührer, A. Schuster, M. Toepfker, B. Haid, E. Wenzl, F. Offner, Intra-operative sonography: a valuable aid during breast-conserving surgery for occult breast cancer., *Ann. Surg. Oncol.* 14 (2007) 3090–101. doi:10.1245/s10434-007-9490-9.
- [57] C.C. Yu, K.C. Chiang, W.L. Kuo, S.C. Shen, Y.F. Lo, S.C. Chen, Low re-excision rate for positive margins in patients treated with ultrasound-guided breast-conserving surgery, *Breast.* 22 (2013) 698–702. doi:10.1016/j.breast.2012.12.019.
- [58] G. Karadeniz Cakmak, A.U. Emre, O. Tascilar, B. Bahadir, S. Ozkan, Surgeon performed continuous intraoperative ultrasound guidance decreases re-excisions and mastectomy rates in breast cancer, in: *Breast*, 2017: pp. 23–28. doi:10.1016/j.breast.2017.02.014.
- [59] M. Ahmed, M. Douek, Intra-operative ultrasound versus wire-guided localization in the surgical management of non-palpable breast cancers: systematic review and meta-analysis, *Breast Cancer Res. Treat.* 140 (2013) 435–446. doi:10.1007/s10549-013-2639-2.
- [60] H. Karanlik, I. Ozgur, D. Sahin, M. Fayda, S. Onder, E. Yavuz, Intraoperative ultrasound reduces the need for re-excision in breast-conserving surgery, *World J. Surg. Oncol.* 13 (2015) 321. doi:10.1186/s12957-015-0731-2.
- [61] J.H. Volders, M.H. Haloua, N.M.A. Krekel, V.L. Negenborn, R.H.E. Kolk, A.M.F. Lopes Cardozo, A.M. Bosch, L.M. de Widt-Levert, H. van der Veen, H. Rijna, A.H.M. Taets van Amerongen, K. Józwiak, S. Meijer, M.P. van den Tol, Intraoperative ultrasound guidance in breast-conserving surgery shows superiority in oncological outcome, long-

- term cosmetic and patient-reported outcomes: Final outcomes of a randomized controlled trial (COBALT), *Eur. J. Surg. Oncol.* 43 (2017) 649–657. doi:10.1016/j.ejso.2016.11.004.
- [62] L.F. Smith, I.T. Rubio, R. Henry-Tillman, S. Korourian, V.S. Klimberg, Intraoperative ultrasound-guided breast biopsy, *Am. J. Surg.* 180 (2000) 419–423. doi:10.1016/S0002-9610(00)00500-6.
- [63] S.P. Harlow, D.N. Krag, S.E. Ames, D.L. Weaver, Intraoperative ultrasound localization to guide surgical excision of nonpalpable breast carcinoma, *J. Am. Coll. Surg.* 189 (1999) 241–246. doi:10.1016/S1072-7515(99)00156-8.
- [64] J.H. Volders, M.H. Haloua, N.M. Krekel, S. Meijer, P.M. van den Tol, Current status of ultrasound-guided surgery in the treatment of breast cancer., *World J. Clin. Oncol.* 7 (2016) 44–53. doi:10.5306/wjco.v7.i1.44.
- [65] T. Nagashima, H. Hashimoto, K. Oshida, S. Nakano, N. Tanabe, T. Nikaido, K. Koda, M. Miyazaki, Ultrasound demonstration of mammographically detected microcalcifications in patients with ductal carcinoma in situ of the breast., *Breast Cancer.* 12 (2005) 216–220. doi:10.2325/jbcs.12.216.
- [66] J.W. Jakub, R.J. Gray, A.C. Degnim, J.C. Boughey, M. Gardner, C.E. Cox, Current status of radioactive seed for localization of non palpable breast lesions, *Am. J. Surg.* 199 (2010) 522–528. doi:10.1016/j.amjsurg.2009.05.019.
- [67] R. Rao, A. Moldrem, V. Sarode, J. White, M. Amen, M. Rao, V. Andrews, D. Euhus, L. Radford, M. Ullissey, Experience with seed localization for nonpalpable breast lesions in a public health care system., *Ann. Surg. Oncol.* 17 (2010) 3241–6. doi:10.1245/s10434-010-1139-4.
- [68] G. Mariani, A.E. Giuliano, H.W. Strauss, *Radioguided surgery: a comprehensive team approach*, Springer, New York, 2008.
- [69] L.M. Lamki, A.U. Buzdar, S.E. Singletary, M.G. Rosenblum, V. Bhadkamkar, L. Esparza, D.A. Podoloff, A. Zukiwski, G.N. Hortobagyi, J.L. Murray, Indium-111-labeled B72.3 monoclonal antibody in the detection and staging of breast cancer: a phase I study., *J. Nucl. Med.* 32 (1991) 1326–1332.
- [70] Y. Tang, J. Wang, D.A. Scollard, H. Mondal, C. Holloway, H.J. Kahn, R.M. Reilly, Imaging of HER2/neu-positive BT-474 human breast cancer xenografts in athymic mice using 111In-trastuzumab (Herceptin) Fab fragments, *Nucl. Med. Biol.* 32 (2005) 51–58.

doi:10.1016/j.nucmedbio.2004.08.003.

- [71] K.G. Andersson, M. Rosestedt, Z. Varasteh, M. Malm, M. Sandström, V. Tolmachev, J. Löfblom, S. Ståhl, A. Orlova, Comparative evaluation of ^{111}In -labeled NOTA-conjugated affibody molecules for visualization of HER3 expression in malignant tumors, *Oncol. Rep.* 34 (2015) 1042–1048. doi:10.3892/or.2015.4046.
- [72] S.R. Urva, J.P. Balthasar, Target mediated disposition of T84.66, a monoclonal anti-CEA antibody: Application in the detection of colorectal cancer xenografts, *MAbs.* 2 (2010) 67–72. doi:10.4161/mabs.2.1.10781.
- [73] P.L. Jager, M.A. de Korte, M.N. Lub-de Hooge, A. van Waarde, K.P. Koopmans, P.J. Perik, E.G. de Vries, Molecular imaging: what can be used today, *Cancer Imaging.* 5 (Spec A) (2005) S27–S32. doi:10.1102/1470-7330.2005.0023.
- [74] I.G. Sergides, R.C.T. Austin, M.C. Winslet, Radioimmunodetection: Technical problems and methods of improvement, *Eur. J. Surg. Oncol.* 25 (1999) 529–539. doi:10.1053/ejso.1999.0691.
- [75] B. Selverstone, W.H. Sweet, C. V Robinson, The clinical use of radioactive phosphorus in the surgery of brain tumors, *Ann. Surg.* 130 (1949) 643–651. doi:10.1097/00000658-194910000-00007.
- [76] N. Avril, M. Menzel, J. Dose, M. Schelling, W. Weber, F. Jänicke, W. Nathrath, M. Schwaiger, F. Ja, W. Nathrath, M. Schwaiger, Glucose metabolism of breast cancer assessed by ^{18}F -FDG PET: histologic and immunohistochemical tissue analysis, *J. Nucl. Med.* 42 (2001) 9–16. <http://www.ncbi.nlm.nih.gov/pubmed/11197987>.
- [77] Y. Sanli, S. Kuyumcu, Z.G. Ozkan, G. Işık, H. Karanlık, B. Guzelbey, C. Turkmen, S. Ozel, E. Yavuz, A. Mudun, Increased FDG uptake in breast cancer is associated with prognostic factors, *Ann. Nucl. Med.* 26 (2012) 345–350. doi:10.1007/s12149-012-0579-2.
- [78] D. Groheux, M. Espié, S. Giacchetti, E. Hindié, Performance of FDG PET/CT in the clinical management of breast cancer, *Radiology.* 266 (2013) 388–405. doi:10.1148/radiol.12110853.
- [79] D. Groheux, A. Cochet, O. Humbert, J.-L. Alberini, E. Hindie, D. Mankoff, ^{18}F -FDG PET/CT for staging and restaging of breast cancer, *J. Nucl. Med.* 57 (2016) 17S–26S. doi:10.2967/jnumed.115.157859.
- [80] F. Daghighian, J.C. Mazziotta, E.J. Hoffman, P. Shenderov, B. Eshaghian, S. Siegel, M.E.

- Phelps, Intraoperative beta probe: A device for detecting tissue labeled with positron or electron emitting isotopes during surgery, *Med. Phys.* 21 (1994) 153–157.
- [81] M.P. Tornai, B.E. Patt, J.S. Iwanczyk, C.R. Tull, L.R. MacDonald, E.J. Hoffman, A novel silicon array designed for intraoperative charged particle imaging, *Med. Phys.* 29 (2002) 2529–2540. doi:10.1118/1.1514241.
- [82] S. Yamamoto, K. Matsumoto, S. Sakamoto, K. Tarutani, K. Minato, M. Senda, An intra-operative positron probe with background rejection capability for FDG-guided surgery., *Ann. Nucl. Med.* 19 (2005) 23–28. doi:10.1007/BF02986331.
- [83] S.S. Huh, D. Burdette, E. Chesi, K. Honscheid, H. Kagan, C. Lacasta, G. Llosa, M. Mikuz, S.J. Park, W.L. Rogers, A. Studen, P. Weilhammer, N.H. Clinthorne, A pixelated silicon positron sensitive imaging probe, in: *IEEE Nucl. Sci. Symp. Conf. Rec.*, 2005: pp. 2588–2591. doi:10.1109/NSSMIC.2005.1596867.
- [84] C. Mester, C. Bruschini, P. Magro, N. Demartines, V. Dunet, E. Grigoriev, A. Konoplyannikov, V. Talanov, M. Matter, J.O. Prior, E. Charbon, A handheld probe for β^+ -emitting radiotracer detection in surgery, biopsy and medical diagnostics based on Silicon Photomultipliers, in: *IEEE Nucl. Sci. Symp. Conf. Rec.*, 2012: pp. 253–257. doi:10.1109/NSSMIC.2011.6154491.
- [85] H. Sabet, B.C. Stack, V. V. Nagarkar, A hand-held, intra-operative positron imaging probe for surgical applications, *IEEE Trans. Nucl. Sci.* 62 (2015) 1927–1934. doi:10.1109/TNS.2015.2446434.
- [86] S. Spadola, M.A. Verdier, L. Pinot, C. Esnault, N. Dinu, Y. Charon, M.A. Duval, L. Ménard, Design optimization and performances of an intraoperative positron imaging probe for radioguided cancer surgery, *J. Instrum.* 11 (2016) P12019. doi:10.1088/1748-0221/11/12/P12019.
- [87] A. Russomando, F. Bellini, V. Bocci, F. Collamati, E. De Lucia, R. Faccini, M. Marafini, I. Mattei, G. Chiodi, V. Patera, L. Recchia, A. Sarti, A. Sciubba, E.S. Camillocci, R. Paramatti, C. Voena, R. Donnarumma, C. Mancini-Terracciano, S. Morganti, An intraoperative β -detecting probe for radio-guided surgery in tumour resection, *IEEE Trans. Nucl. Sci.* 63 (2016) 2533–2539. doi:10.1109/TNS.2016.2600266.
- [88] E. Solfaroli Camillocci, V. Bocci, G. Chiodi, F. Collamati, R. Donnarumma, R. Faccini, C. Mancini Terracciano, M. Marafini, I. Mattei, S. Muraro, L. Recchia, A. Rucinski, A.

- Russomando, M. Toppi, G. Traini, S. Morganti, Intraoperative probe detecting β -decays in brain tumour radio-guided surgery, *Nucl. Instruments Methods Phys. Res. Sect. A Accel. Spectrometers, Detect. Assoc. Equip.* 845 (2017) 689–692.
doi:10.1016/j.nima.2016.04.107.
- [89] R.R. Raylman, Performance of a dual, solid-state intraoperative probe system with ^{18}F , $^{99\text{m}}\text{Tc}$, and $(^{111})\text{In}$., *J. Nucl. Med.* 42 (2001) 352–360.
- [90] P. Ervin B., *Radiation Physics for Medical Physicists*, Second, Springer, 2009.
- [91] G. Knoll, *Radiation Detection and Measurement*, Wiley. (2005).
- [92] M.P. Tornai, *Small area beta and gamma detectors for functional nuclear emission imaging*, University Of California Los Angeles, 1997.
- [93] Sensl, *An introduction to the silicon photomultiplier*, (2011).
<https://www.sensl.com/downloads/ds/TN - Intro to SPM Tech.pdf>.
- [94] Sensl, *Low noise, blue-sensitive silicon photomultipliers*, (2014).
<http://sensl.com/downloads/ds/DS-MicroCseries.pdf> (accessed April 1, 2018).
- [95] C.S. Levin, L.R. MacDonald, M.P. Tornai, E.J. Hoffman, J. Park, Optimizing light collection from thin scintillators used in a beta-ray camera for surgical use, *IEEE Trans. Nucl. Sci.* 43 (1996) 2053–2060. doi:10.1109/23.507268.
- [96] S.R. Cherry, Y. Shao, M.P. Tornai, S. Siegel, A.R. Ricci, M.E. Phelps, Collection of scintillation light from small BGO crystals, *IEEE Trans. Nucl. Sci.* 42 (1995) 1058–1063. doi:10.1109/23.467749.
- [97] E. Tornai, M.P. Levin, C.S. MacDonald, L.R. Hoffman, Investigation of crystal geometries for fibre coupled gamma imaging intraoperative probe, *IEEE Trans. Nucl. Sci.* 44 (1995) 1254–1261. doi:10.1109/23.596997.
- [98] Canadian Institute for Health Information, *Breast Cancer Surgery in Canada*, by Province/Territory, 2008–2009 to 2013–2014, (2016).
https://www.cihi.ca/sites/default/files/document/quickstat_breastcancer_en_1.xlsm%0A (accessed December 11, 2017).
- [99] M.J. Dryden, B.E. Dogan, P. Fox, C. Wang, D.M. Black, K. Hunt, W.T. Yang, Imaging factors that influence surgical margins after preoperative ^{125}I radioactive seed localization of breast lesions: Comparison with wire localization, *Am. J. Roentgenol.* 206 (2016) 1112–1118. doi:10.2214/AJR.15.14715.

- [100] B. Pouw, L.J. De Wit-Van Der Veen, M.P.M. Stokkel, C.E. Loo, M.J.T.F.D. Vrancken Peeters, R.A. Vald??s Olmos, Heading toward radioactive seed localization in non-palpable breast cancer surgery? A meta-analysis, *J. Surg. Oncol.* 111 (2015) 185–191. doi:10.1002/jso.23785.
- [101] A. Ravi, *Gamma-ray detector guidance of breast cancer therapy*, University of Toronto, 2009.
- [102] I. Holl, E. Loren, G. Mageras, A measurement of the light yield of common inorganic scintillators, *IEEE Trans. Nucl. Sci.* 35 (1988) 105–109. doi:10.1109/23.12684.
- [103] P. Dorenbos, J.T.D. de Haas, C.W.V. van Eijk, Non-proportionality in the scintillation response and the energy resolution obtainable with scintillation crystals, *IEEE Trans. Nucl. Sci.* 42 (1995) 2190–2202. doi:10.1109/23.489415.
- [104] D.T. Geddes, Inside the lactating breast: The latest anatomy research, *J. Midwifery Women’s Heal.* 52 (2007) 556–563. doi:10.1016/j.jmwh.2007.05.004.
- [105] NIST, ESTAR : Stopping Power and Range Tables for Electrons, (2017). https://physics.nist.gov/cgi-bin/Star/e_table.pl (accessed February 21, 2018).
- [106] L.A. Currie, Limits for qualitative detection and quantitative determination: Application to radiochemistry, *Anal. Chem.* 40 (1968) 586–593. doi:10.1021/ac60259a007.
- [107] S. Zincirkeser, E. Sahin, M. Halac, S. Sager, Standardized uptake values of normal organs on 18F-fluorodeoxyglucose positron emission tomography and computed tomography imaging., *J. Int. Med. Res.* 35 (2007) 231–236.
- [108] A.A. Zytoon, Standardized uptake value variations of normal glandular breast tissue at dual time point FDG-PET/CT imaging, *Int. J. Med. Imaging.* 1 (2013) 56–65. doi:doi: 10.11648/j.ijmi.20130103.14.
- [109] R. Kumar, A. Chauhan, H. Zhuang, P. Chandra, M. Schnall, A. Alavi, Standardized uptake values of normal breast tissue with 2-deoxy-2-[F-18]fluoro-D: -glucose positron emission tomography: variations with age, breast density, and menopausal status, *Mol. Imaging Biol.* 8 (2006) 355–362. doi:10.1007/s11307-006-0060-5.
- [110] D. Vranjesevic, C. Schiepers, D.H. Silverman, A. Quon, J. Villalpando, M. Dahlbom, M.E. Phelps, J. Czernin, Relationship between 18F-FDG uptake and breast density in women with normal breast tissue, *J. Nucl. Med.* 44 (2003) 1238–42. <http://www.ncbi.nlm.nih.gov/pubmed/12902413>.

- [111] S. Basu, A. Mavi, T. Cermik, M. Houseni, A. Alavi, Implications of standardized uptake value measurements of the primary lesions in proven cases of breast carcinoma with different degree of disease burden at diagnosis: Does 2-Deoxy-2-[F-18]fluoro-d-glucose-positron emission tomography predict tumor biolog, *Mol. Imaging Biol.* 10 (2008) 62–66. doi:10.1007/s11307-007-0121-4.
- [112] A. Azuma, M. Tozaki, K. Ito, E. Fukuma, T. Tanaka, T. O’Uchi, Ductal carcinoma in situ: Correlation between FDG-PET/CT and histopathology, *Radiat. Med. - Med. Imaging Radiat. Oncol.* 26 (2008) 488–493. doi:10.1007/s11604-008-0263-6.
- [113] U. Tateishi, T. Terauchi, S. Akashi-Tanaka, T. Kinoshita, D. Kano, H. Daisaki, T. Murano, H. Tsuda, H.A. Macapinlac, Comparative study of the value of dual tracer PET/CT in evaluating breast cancer, *Cancer Sci.* 103 (2012) 1701–1707. doi:10.1111/j.1349-7006.2012.02348.x.
- [114] B.B. Koolen, F. Van Der Leij, W. V. Vogel, E.J.T. Rutgers, M.J.T.F.D. Vrancken Peeters, P.H.M. Elkhuisen, R.A. Valdés Olmos, Accuracy of 18F-FDG PET/CT for primary tumor visualization and staging in T1 breast cancer, *Acta Oncol. (Madr).* 53 (2014) 50–57. doi:10.3109/0284186X.2013.783714.
- [115] C. Mancini-Terracciano, R. Donnarumma, G. Bencivenga, V. Bocci, A. Cartoni, F. Collamati, I. Fratoddi, A. Giordano, L. Indovina, D. Maccora, M. Marafini, R. Mirabelli, S. Morganti, D. Rotili, A. Russomando, T. Scotognella, E. Solfaroli Camillocci, M. Toppi, G. Traini, I. Venditti, R. Faccini, Feasibility of beta-particle radioguided surgery for a variety of “nuclear medicine” radionuclides, *Phys. Medica.* 43 (2017) 127–133. doi:10.1016/j.ejmp.2017.10.012.
- [116] M. Angelone, G. Battistoni, F. Bellini, V. Bocci, F. Collamati, E. De Lucia, R. Faccini, F. Ferroni, S. Fiore, M. Marafini, D. Materazzo, I. Mattei, S. Morganti, V. Patera, L. Piersanti, M. Pillon, L. Recchia, A. Russomando, A. Sarti, A. Sciubba, E. Solfaroli Camillocci, C. Voena, Properties of para-terphenyl as a detector for α , β and γ radiation, *IEEE Trans. Nucl. Sci.* 61 (2014) 1483–1487. doi:10.1109/TNS.2014.2322106.
- [117] H. Wong, S. Lau, T. Yau, P. Cheung, R.J. Epstein, Presence of an in situ component is associated with reduced biological aggressiveness of size-matched invasive breast cancer, *Br. J. Cancer.* 102 (2010) 1396. doi:10.1038/sj.bjc.6605655.